LIQUID CRYSTAL PHASE TRANSITIONS IN DISPERSIONS OF RODLIKE COLLOIDAL PARTICLES

H.N.W. LEKKERKERKER, P. BUINING, J. BUITENHUIS,
G.J. VROEGE AND A. STROOBANTS
Van 't Hoff Laboratory for Physical and Colloid Chemistry
Utrecht University
Padualaan 8, 3584 CH Utrecht, The Netherlands

1. Introduction and Overview

Dispersions are called colloidal when the dispersed particles are larger than common small molecules, say larger than 1 nm, but small enough not to show appreciable sedimentation in normal gravity, say smaller than 1 μm. Colloidal particles are equivalent to molecules and atoms in that they undergo thermal motion. When the particles are monodisperse i.e. all particles have the same or nearly the same size, the colloidal system will exhibit a far-reaching resemblance in its statistical behaviour to atomic and molecular systems. In fact the equilibrium statistical thermodynamic properties of colloidal dispersions may be treated in exactly the same way as in the case of simple liquids by considering the colloidal particles as "supramolecules" in a continuous (but fluctuating) back-ground. The potential which for the case of fluctuating forces replaces the interaction potential between molecules (in vacuo) is the potential of the average forces which act between the dispersed particles, also denoted as potential of mean force. This effective interaction is the input for statistical mechanical theories. Therefore statistical mechanical theories developed for atomic fluids and solids can be applied to colloidal dispersions. The theoretical basis for such a treatment was given by Onsager [1,2,3] and McMillan and Mayer [4].

One of the most remarkable phenomena exhibited by concentrated suspensions of colloidal particles is the spontaneous transition from fluid-like structures in which there are only short-range correlations between the positions and orientations of the particles to structures which have long-range spatial and/or orientational order. Such a transition was first observed and

M. Baus et al. (eds.), Observation, Prediction and Simulation of Phase Transitions in Complex Fluids, 53–112.

recognized as such by Zocher [20] in suspensions of rod-like colloidal V_2O_5 particles where, at a volume fraction of a few percent an isotropic-nematic phase transition occurs. Later more extensive studies of this phase transition were performed on dispersions of tobacco mosaic virus (TMV) [21-23], a rod-like particle with length L = 300 nm and diameter D = 18 nm. A similar disorder-to-order transition was observed early on by Langmuir [24] in a dispersion of plate-like particles (colloidal bentonite particles). As early as 1939 Best [25] studied TMV dispersions as a function of added salt and found that the isotropic-nematic phase transition shifts to lower concentrations upon lowering the salt concentration. This means that strengthening the repulsive interaction between the particles shifts the phase transition to lower concentrations. This may appear to go against the common notions about phase transitions, where it is usually assumed that some attractive interaction is necessary for the coexistence of two phases with different densities and/or concentrations. Onsager [2,3] however, clearly showed that the isotropic-nematic phase transition in dispersions of rod-like particles can be explained without invoking any attractive interactions. The transition can be understood on the basis of a competition between orientational entropy favouring the isotropic phase versus the excluded-volume entropy favouring the nematic phase. This gave rise to the concept of entropic phase separation.

Colloidal liquid crystals have been studied most extensively in suspensions of rod-like virus particles such as TMV (see the lectures of S. Fraden). In the Van 't Hoff Laboratory we have worked over the last years on the development of a new model system of colloidal rod-like particles. The particles consist of a core of γ-A100H (Boehmite) [41,42] and are sterically stabilized by a layer of polyisobutene (with a molecular weight of 1300 and a resulting thickness of the sterical stabilization layer of about 4 nm) [43]. It was hoped to obtain a system that could play for colloidal liquid crystal phase transitions a similar role as the (almost) "hard-sphere" colloids developed over the last 15 years [14,15] have played for colloidal crystal phase transitions (see the lectures of P.N. Pusey and W.C.K. Poon). Although the systems we have been able to make so far are not as perfectly shaped as TMV, we nevertheless have been able to observe interesting (liquid crystal) phase transition phenomena with these systems which-together with the relevant theoretical background-are discussed in these lectures.

2. Special Features of Phase Transitions in Colloidal Systems.

We will first discuss the characteristic features of phase transitions in colloidal systems that make them special compared to the usual phase transitions in atomic and molecular systems. In figure 1 we give a schematic

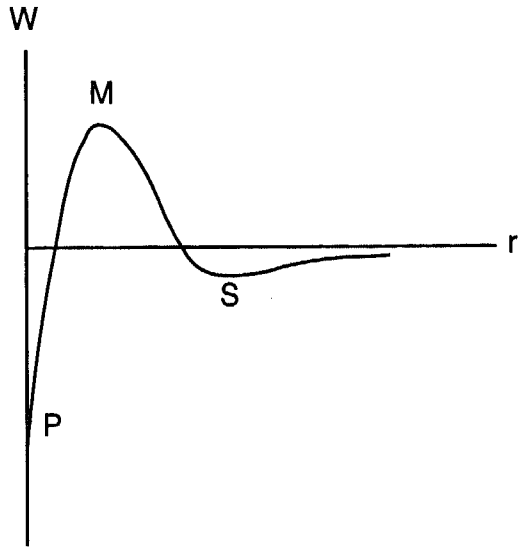

Figure 1. Schematic plot of the potential of average force, W(r), for electric double layer repulsion plus Van der Waals attraction forces showing the primary minimum P, the maximum M and the secondary minimum S.

plot of the now classical Derjaguin-Landau-Verwey-Overbeek potential of mean force $W(r)$ between two hydrophobic colloids which is determined by electrical double layer repulsion and Van der Waals attraction [5,6].

$$W_{DLVO}(r) = -\frac{A}{12}h(x) + B\frac{\exp(-\kappa(x-1))}{x} \qquad (1)$$

The first term on the right-hand side of eq. (1) is due to the Van der Waals attraction between the colloidal particles (in the suspension medium) with A the Hamaker constant (typically of order 10^{-20}J) and h a function of the distance between the particles

$$h(x) = \left[\frac{1}{x^2-1} + \frac{1}{x^2} + 2\ln\left(1-\frac{1}{x^2}\right)\right]$$

with $x = r/\sigma$ the dimensionless distance between the particles (r: distance between the centres of the colloidal spheres, σ: diameter of the colloidal spheres). The second term on the right-hand side of eq. (1) is due to the repulsion of the electric double layers of the particles. The amplitude B (typically of order 10^{-18}J) depends on the surface charge/potential of the

colloidal particles and $\kappa = \sigma/\xi$ is the dimensionless Debye screening constant (ξ: Debye length).

Generally $W(r)$ has two minima separated by a maximum depending on the surface potential of the particles and the electrolyte content. If the maximum is too low or absent two interacting particles may reach the primary minimum leading to "irreversible" aggregation[1]. Since hydrophobic colloids are not equilibrium systems in the thermodynamic sense the problem of the stability of hydrophobic colloids is essentially one of the kinetics of the "irreversible" aggregation process. Unstable colloidal dispersions ordinarily form relatively concentrated flocs which separate from the continuous medium. "Irreversible" aggregation can be seen as a phase separation process in the deep quench limit when separation proceeds only along a path of decreasing internal energy and cluster breaking is very rare [8]. The observations of "irreversible" aggregation in hydrophobic colloids have contributed to the feeling in the early days of colloid science that thermodynamic criteria of stability could not be applied to colloids.

This situation changed with the possibility to prepare stable dispersions of highly monodisperse microspheres of synthetic polymers (latex particles) with concentrations up to 0.6 in volume fraction. In the sixties and seventies a number of studies appeared on the transition from the milky white disordered state (colloidal fluid) to the iridescent ordered state (colloidal crystal) [9-11]. At first it was thought that this fluid-crystal transition was caused by condensation in the secondary minimum of the DLVO potential. However the experiments of Hachisu et al. [11] gave strong objections to this interpretation. They studied the conditions for the formation of the ordered phase by changing the ionic concentration and the latex particle concentration. By lowering the ionic concentration they could observe the ordered phase at surprisingly low concentrations of the latex particles (as low as 0.01% by volume fraction). This means that strengthening of the repulsive interaction produces the disorder-to-order transition. This seems contradictory to the common intuition that some attractive interaction is necessary for the coexistence of two phases with different density. This difficulty is solved by invoking the concept of the Kirkwood-Alder hard sphere fluid-crystal transition [12-15] as was first done by Wadati and Toda [16]. As early as 1939 Kirkwood [12] speculated that in a system of hard spheres there is a certain limiting density above which a liquid type of structure cannot exist but only structures with crystalline long-range order. This prediction became only respectable when it was confirmed by the Monte Carlo simulations of Wood and Jacobson [13] and the Molecular Dynamics Cal-

[1]In fact in a large number of cases colloidal particules aggregated in the primary minimum can be redispersed[7]. Therefore strictly speaking it is not correct to denote aggregation in the primary minimum as irreversible aggregation.

culations of Alder and Wainwright [14]. The transition can be understood on the basis of a competition between two forms of entropy: a loss in ideal (non-interacting) entropy when the particles go into the ordered state and a gain in packing (excluded-volume) entropy resulting from particle localization. Employing this theory the phase behaviour of latex is explained as follows. Latex with a repulsive interaction is equivalent to a hard sphere system, the hard sphere being larger than the actual latex particles, and the fluid-crystal transition occurs at volume fractions below 0.5 predicted for the hard sphere freezing transition. At electrolyte concentrations of about 0.1 M the effective range of the interparticle interaction is reduced to a small fraction of the particle diameter. The particles then behave as nearly hard spheres and the phase transition now occurs at volume fractions in the range 0.5-0.55 in close agreement with the coexistence volume fractions obtained by computer simulations for the hard sphere fluid-solid transition [15]. Over the last decade it has become possible to prepare (almost) monodisperse spherical colloidal particles with short chains grafted on their surface whose short-ranged harshly repulsive interparticle forces closely approximate that of hard spheres [17,18]. The observed phase behaviour is in good agreement with the theoretical values for the volume fractions for freezing and melting in a hard sphere system [19]. In the case of atomic and molecular systems it is possible by rapid cooling to bypass crystallization and bring the system in an amorphous (glassy) state. Similarly in colloidal systems sufficiently rapid densification leads to the formation of an amorphous (glassy) sediment that may not crystallize for (many) years. Generally mild centrifugation or just sedimentation under the earth gravity provides already sufficiently rapid densification.

So far we have discussed disorder-to-order transitions under the influence of repulsive interactions. Of course attractive interactions are present in colloidal systems and we want to discuss why, notwithstanding their presence, the equivalent of gas-liquid phase transitions are so rarely observed in colloidal dispersions. In order to appreciate this special feature of phase transitions in colloidal systems let us first consider the phase behaviour of simple atomic systems (such as argon) whose interactions can be adequately described in terms of simple pair potentials such as the well known Lennard-Jones potential.

$$V_{LJ}(r) = 4\varepsilon\left[\left(\frac{\sigma}{r}\right)^{12} - \left(\frac{\sigma}{r}\right)^{6}\right] \tag{2}$$

The minimum of this potential is $-\varepsilon$ and is reached for $r_{min} = 2^{1/6}\sigma \cong 1.12\sigma$. To quantify the range of the attractive part of the above potential we introduce the parameter

$$\delta = \frac{r_1 - r_{min}}{r_{min}}$$

where r_1 is the value of $r > r_{min}$ for which $V_{LJ}(r)$ attains one-percent of its value at the minimum. A simple calculation yields $r_1 \cong 2.71\sigma$ and thus $\delta = 1.42$ indicating that the range of the attraction is at least comparable to or larger than the range of the repulsion.

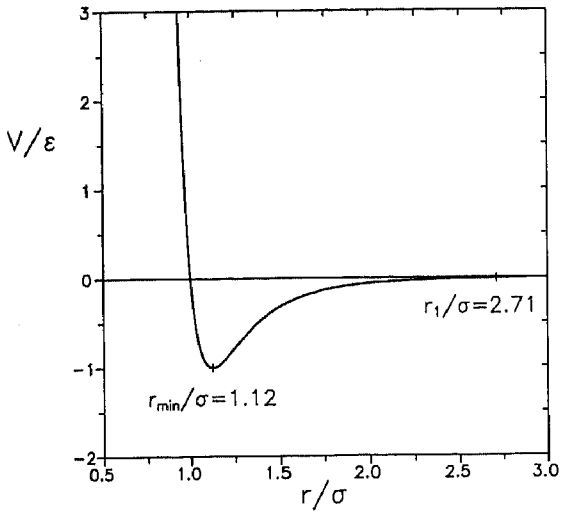

Figure 2. Lennard Jones potential. Indicated are the minimum and the value r_1/σ for which $\frac{V_{LJ}(r_1/\sigma)}{\epsilon} = -0.01$.

The phase behaviour of atomic systems described by Lennard-Jones systems has been studied extensively [26]. The phase diagram (see figure 3) in the temperature-density plane has a face-centered-cubic solid at high densities and a gas-liquid envelope at intermediate densities and temperatures bounded by the critical point and the triple line.

In fig. 4 we compare the LJ potential with the DLVO potential for a stable colloidal particle (i.e. the maximum is large enough to prevent "irreversible" aggregation). The interaction energy is expressed in units of the well depth ε in the case of the LJ potential and the depth of the secondary minimum in the case of the DLVO potential. On this scale the top of the maximum and the primary minimum are outside the range of the diagram.

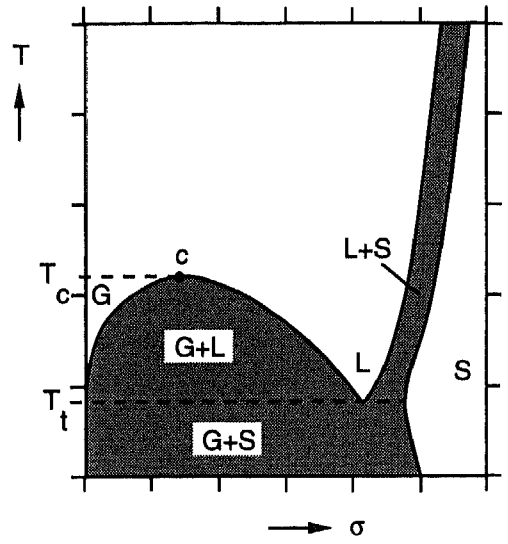

Figure 3. Schematic representation of the temperature-density phase diagram of the Lennard-Jones system.

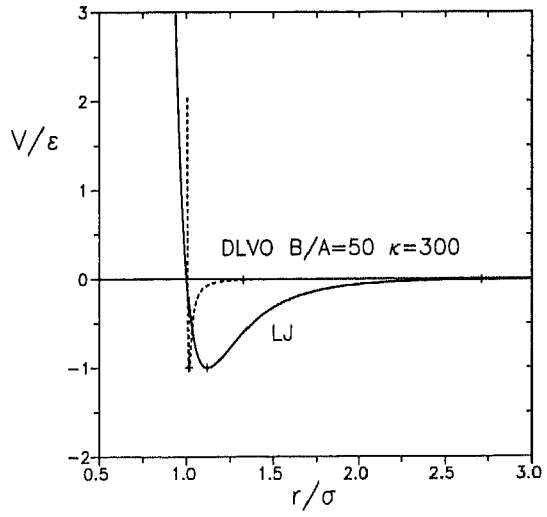

Figure 4. A comparison of the Lennard-Jones potential that describes the pair interaction of noble gases (solid line) and the Derjaguin-Landau-Verwey-Overbeek potential that describes the interaction of charge-stabilized colloidal particles.(dotted line)

A striking feature of the DLVO potential is that the range of the attraction (relative to the hard core) is very small compared to that of the LJ potential. A number of authors [27-30] have considered the possibility that the reversible aggregation in the secondary minimum may lead to a phase separation of the condensation type (i.e. gas-liquid or gas-solid). Over the last decade it has become clear [31-36] that when the range of the attraction is less than about one third of the diameter of the hard core of the particles the gas-liquid transition becomes metastable with respect to the fluid-solid transition (see fig.5).

In order to understand the implications of fig. 5 for phase transitions in colloidal systems one has to realize that the value of W/kT changes over a much wider range by changes in the electrolyte concentration than by a change in temperature T. Roughly speaking the high temperature part of the phase diagram corresponds to low electrolyte concentration and the low temperature part to high electrolyte concentration (but still low enough to avoid normal coagulation). On the basis of the present insights concerning the effect of the range of the attraction on the phase behaviour a gas-liquid transition in a charge-stabilized colloidal system due to the secondary minimum almost seems to be excluded. Experimentally it is not easy to distinguish the gas-liquid and gas-solid transition as the narrow deep attraction gives rise to metastable liquid-like clusters (see e.g. ref. 37) which we believe are in fact precursors of the solid phase. The latter phase which, due to the narrow attraction, occurs at densities near close packing will hardly ever reach its equilibrium state.

In the case of colloids sterically stabilized by grafted chains, the interaction forces are frequently dominated by the chain-chain and chain-solvent interactions. At certain temperatures there may be a preferential solvation of chain segments by other chain segments instead of solvent molecules, which results in an effective attraction force when two opposing particle surface layers approach each other. The range of these attractive forces is roughly of the order of the chain length and thus generally much smaller than the size of the core of the colloidal particles. At the same time the depth of these attractive interactions, being the result of the interaction of many grafted chains, may be many times kT. Under these conditions what may seem to be a gas-liquid transition [38] is in fact (reversible) gelation [39].

A convenient way to vary the range and depth of the attractive part of the potential of mean force between colloidal particles is the addition of non-adsorbing polymer. The attraction in this case is caused by the exclusion of polymer from the region in between two colloid particles when their surface-surface separation becomes smaller than the diameter of a free polymer coil. The resulting imbalance in osmotic pressure gives rise to an

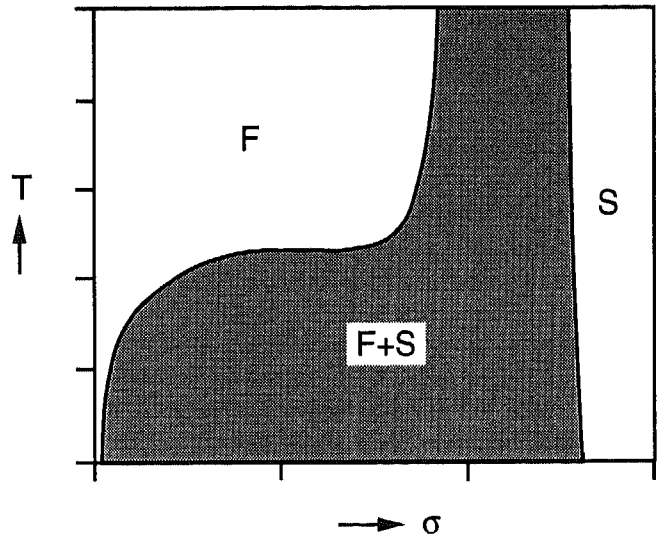

Figure 5. Schematic representation of the phase diagram for particles with a narrow attraction.

effective attractive depletion force between the colloid particles. Here the range of the attraction is directly related to the size of the added polymer and the strength is related to its concentration. By tuning the range of the attractive potential it is possible to observe two phases (colloidal fluid and crystal) or three phases (colloidal gas, liquid and crystal) [31-33,40].

3. Statistical Mechanics of Colloidal Dispersions. Potential of Mean Force

The analogy between the statistical physics of atomic systems and colloidal dispersions was in fact already exploited by Jean Perrin [44] in the first decade of this century in his fundamental investigations on Brownian motion and sedimentation equilibrium. The experiments of Perrin were carried out on dilute dispersions such that interaction effects generally could be neglected. However, already Perrin [45] and Constantin [46] noted that in some cases sedimentation equilibria could be described better by using an (osmotic) equation of state that incorporated interaction effects. In recent years concepts of liquid state theory have been applied systematically and succesfully to understand the behaviour of concentrated colloidal dispersions [47].

The formal basis for the far-reaching analogy between the statistical physics of colloidal dispersions and atomic systems is provided by the fact

that the equilibrium statistical mechanics of both types of systems becomes completely equivalent when the bare interaction potential for the case of atoms is replaced by the potential which is derived from the average of all forces acting upon the colloid particles for the case of dispersions [1-4]. Since this potential of mean force is an important concept in the application of statistical mechanics of phase transitions to colloidal dispersions we consider here some of its fundamental aspects.

Consider a suspension consisting of N colloidal particles dispersed in a solvent (component 0) that may also contain further species such as ions, polymer molecules, ... (components a,b,...) in an osmotic cell with volume V in dialytic equilibrium with a reservoir solely containing the solvent components 0, a, b, ... Denoting the hydrostatic pressures in the cell and the reservoir by P and P^R respectively, the osmotic pressure difference Π between the cell and the reservoir is given by

$$\Pi = P - P^R \tag{3}$$

Since the dispersion may be considered an open system with respect to the solvent molecules, the appropriate (configurational) partition function for the colloidal dispersion in the osmotic cell is

$$\Xi(N,V,T,\mu_0) = \sum_{N_0 \geq 0} z_0^{N_0} Z(N,V,T,N_0) \tag{4}$$

Here z_0 is the activity of the solvent which is related to its chemical potential μ_0 (we consider here the case that the solvent contains one component, the generalization to situations with several solvent components is straightforward)

$$z_0 = \exp(\mu_0/kT) \tag{5}$$

and $Z(N,V,T,N_0)$ is the canonical configurational partition function

$$Z(N,V,T,N_0) = \frac{1}{N!N_0!} \int e^{-U(\vec{r}^N,\vec{r}^{N_0})/kT} d\vec{r}^N d\vec{r}^{N_0} \tag{6}$$

Here $\vec{r}^N$ and $\vec{r}^{N_0}$ denote the positions of the N colloidal particles and the N_0 solvent molecules and $U(\vec{r}^N,\vec{r}^{N_0})$ is the interaction potential of the N colloidal particles and N_0 solvent molecules. The potential of the average forces $W(\vec{r}^N;\mu_0)$ is introduced by writing the (semi)grand canonical partition function in the form

$$\Xi(N,V,T,\mu_0) = \frac{1}{N!}\int e^{-W(\vec{r}^N;\mu_0)/kT}d\vec{r}^N \tag{7}$$

Comparing eqs. (4), (6) and (7) it follows that one can write

$$\exp(-W(\vec{r}^N;\mu_0)/kT) = \sum_{N_0\geq 0}\frac{z_0^{N_0}}{N_0!}\int e^{-U(\vec{r}^N,\vec{r}^{N_0})/kT}d\vec{r}^{N_0} \tag{8}$$

The origin of the name potential of mean force that is commonly used for $W(\vec{r}^N;\mu_0)$ becomes evident by considering the average force on the colloidal particle j in the osmotic cell for a given configuration of colloidal particles

$$< \vec{F}_j >= \frac{\sum_{N_0\geq 0}\frac{Z_0^{N_0}}{N_0!}\int\left(-\frac{\partial U}{\partial \vec{r}_j}\right)\exp(-U/kT)d\vec{r}^{N_0}}{\sum_{N_0\geq 0}\frac{Z_0^{N_0}}{N_0!}\int\exp(-U/kT)d\vec{r}^{N_0}} = -\frac{\partial W}{\partial \vec{r}_j} \tag{9}$$

From $\Xi(N,V,T,\mu_0)$ one can calculate the (semi)grand potential of the colloidal dispersion in the osmotic cell

$$\Omega(N,V,T,\mu_0) = -kT\ln\Xi(N,V,T,\mu_0) \tag{10}$$

In order to focus on the colloidal component it is convenient to subtract from this quantity the grand potential of the solvent $\Omega(V,T,\mu_0) = -P^R V$. We then have

$$\begin{aligned}\Delta\Omega(N,V,T,\mu_0) &= \Omega(dispersion) - \Omega(solvent)\\ &= \Omega(N,V,T,\mu_0) + P^R V\end{aligned} \tag{11}$$

The term $-P^R V$ can also be incorporated in the potential of mean force

$$\Delta W(\vec{r}^N;\mu_0) = W(\vec{r}^N;\mu_0) - (-P^R V) \tag{12}$$

Then we can write

$$\Delta\Omega(N,V,T,\mu_0) = -kT\ln\left\{\frac{1}{N!}\int\exp(-\Delta W(\vec{r}^N;\mu_0)/kT)d\vec{r}^N\right\} \tag{13}$$

Now the analogy between colloidal dispersions and atomic fluids is complete if one uses for the colloidal dispersion $\Delta\Omega(N,V,T,\mu_0)$ where one would have used the Helmholtz free energy $F(N,V,T)$ for an atomic fluid. For example the thermodynamic relation

$$-\left(\frac{\partial F}{\partial V}\right)_{N,T} = P \tag{14}$$

which gives the pressure for an atomic fluid is replaced by

$$-\left(\frac{\partial \Delta\Omega}{\partial V}\right)_{N,T,\mu_0} = P - P^R = \Pi \tag{15}$$

which gives the osmotic pressure. For dilute dispersions $\Delta W \to 0$ and the osmotic pressure is given by Van 't Hoff's law

$$\Pi = \frac{N}{V}kT \tag{16}$$

which is the equivalent of the ideal gas law for an atomic system. McMillan and Mayer [4] have shown how the virial expansion for the osmotic pressure can be obtained starting from the potential of mean force approach.

We would like to emphasize that the solvent in osmotic equilibrium with the colloidal dispersion will in general not have the same composition as the solvent in the colloidal dispersion. This can be seen by taking the derivative of the grand potential of the colloidal dispersion and the equilibrium solvent with respect to the chemical potential of the solvent

$$\frac{< N_0 >}{V}(dispersion) = -\frac{1}{V}\left(\frac{\partial\Omega(dispersion)}{\partial\mu_0}\right)_{N,V,T} \tag{17}$$

$$\frac{< N_0 >}{V}(solvent) = -\frac{1}{V}\left(\frac{\partial\Omega(solvent)}{\partial\mu_0}\right)_{V,T} = \left(\frac{\partial P^R}{\partial\mu_0}\right)_T \tag{18}$$

From eq. (8) it is clear that $W(\vec{r}^N;\mu_0)$ can be considered as the grand potential of the solvent with N colloidal particles embedded in it at fixed positions $\vec{r}^N$. This constitutes a (strongly) inhomogeneous system with a large interfacial area and obviously the calculation of W is not an easy problem. However from the late thirties on progress has been made with as landmark the evaluation of the potential of mean force for charged colloidal particles independently by Derjaguin and Landau [5] in Russia and Verwey and Overbeek [6] in the Netherlands.

After having elucidated the meaning of the potential of mean force and its relation to $\Delta\Omega(N,V,T,\mu_0)$ we will conform to common practice in the rest of this paper. This means that we not always explicitly mention the constancy of the chemical potential of the solvent, μ_o. However, it is always implied that a potential of mean force should be used instead of a bare potential. Finally, we will further use the symbol F for the free energy of the solute components, which is denoted by $\Delta\Omega(N,V,T,\mu_0)$ in the foregoing. Therefore the pressure derived from this free energy is actually the osmotic pressure as defined in eq. (15).

4. The Isotropic-Nematic Transition in Monodisperse Suspensions of Thin Hard Rods

The idea that the statistical thermodynamics of a colloidal dispersion can be treated in a completely analogous way to that of an atomic or molecular system was exploited by Onsager [2,3] in his virial theory of the isotropic-nematic phase transition in a dispersion of long rigid hard rods. The appropriate free energy of N rigid hard rods with length L and diameter D $(L/D >> 1)$ in a dispersion volume V can be expanded in a virial series

$$\frac{F(N,V,T,[f])}{NkT} = constant + \ln\rho + \sigma[f] + B_2([f])\rho + \frac{1}{2}B_3([f])\rho^2 + \ldots \quad (19)$$

Here $\rho = N/V$ is the number density of the rods. Further $f(\vec{a})$ is the orientation distribution function which gives the probability of finding a rod with an orientation in the direction characterized by the unit vector $\vec{a}$. This distribution function must be normalized

$$\int f(\vec{a})d\Omega(\vec{a}) \;=\; 1 \quad (20)$$

where $d\Omega(\vec{a})$ is the element of solid angle surrounding the direction $\vec{a}$.

In the isotropic phase all directions are equally probable which implies in view of the normalization condition (20)

$$f_{iso}(\vec{a}) \;=\; \frac{1}{4\pi} \quad (21)$$

In the nematic phase we must take into account that the orientational distribution function is non-uniform. As a consequence of this non-uniform $f(\vec{a})$ in the nematic phase we must subtract from F an orientational entropy

$$S_{or} = -Nk\int f(\vec{a})\ln[4\pi f(\vec{a})]d\Omega = -Nk\sigma[f] \quad (22)$$

multiplied by T.

The osmotic virial coefficients B_n can be expressed in terms of the irreducible cluster integrals [4] β_{n-1}, assuming that the potential of mean force can be written as a sum of pairwise additive contributions w(i,j)

$$\beta_1(\vec{a}_1,\vec{a}_2) = \frac{1}{V}\int \Phi(1,2)d\vec{r}_1 d\vec{r}_2 \tag{23}$$

$$\beta_2(\vec{a}_1,\vec{a}_2,\vec{a}_3) = \frac{1}{2V}\int \Phi(1,2)\Phi(1,3)\Phi(2,3)d\vec{r}_1 d\vec{r}_2 d\vec{r}_3 \tag{24}$$

Here $\Phi(i,j)$ denotes the Mayer function, which has the usual form but with the bare pair potential $u(i,j)$ replaced by $w(i,j)$

$$\Phi(i,j) = \exp(-w(i,j)/kT) - 1 \tag{25}$$

The cluster integrals, which obviously depend on the orientations of the particles through w, must be orientationally averaged to obtain the virial coefficients

$$B_2 = -\frac{1}{2}\int \beta_1(\vec{a}_1,\vec{a}_2)f(\vec{a}_1)f(\vec{a}_2)d\Omega_1 d\Omega_2 \tag{26}$$

$$B_3 = -\frac{2}{3}\int \beta_2(\vec{a}_1,\vec{a}_2,\vec{a}_3)f(\vec{a}_1)f(\vec{a}_2)f(\vec{a}_3)d\Omega_1 d\Omega_2 d\Omega_3 \tag{27}$$

Since the potential of mean force depends on the chemical potential of the solvent, the osmotic virial coefficients in principle also depend on it. Here we consider hard rods which are characterized by particularly simple potentials and Mayer functions

$w = \infty \quad \Phi = -1$ for overlapping particles
$w = 0 \quad \Phi = 0$ for non-overlapping particles

This makes the cluster integral β_1 the negative of the excluded volume v_{excl} of two rods.

$$\beta_1(\vec{a}_1,\vec{a}_2) = \frac{1}{V}\int \Phi(1,2)d\vec{r}_1 d\vec{r}_2 = \int_{overlap}(-1)d\vec{r}_{12} = -v_{excl}(\vec{a}_1,\vec{a}_2) \tag{28}$$

As a model for hard rods we may take spherocylinders (consisting of cylinders of diameter D and length L capped with two hemispheres). The volume excluded to a second spherocylinder due to the presence of the first is sketched in fig. 6 and is dependent on the angle $\gamma(\vec{a}_1,\vec{a}_2)$ between both cylinders

$$-\beta_1(\vec{a}_1,\vec{a}_2) = 2L^2D|\sin\gamma| + 2\pi D^2 L + \frac{4}{3}\pi D^3 \tag{29}$$

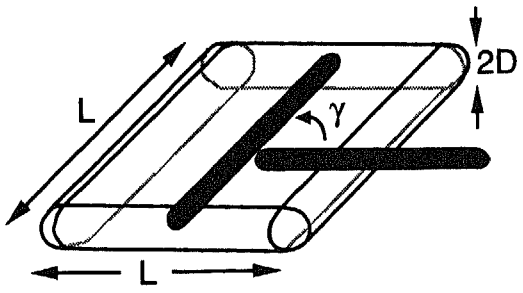

Figure 6. The excluded volume of two spherocylinders.

Note that the last two terms are end corrections which are of order D/L smaller than the leading term. For thin rods these end effects are of minor importance, thus giving

$$-\beta_1(\vec{a}_1, \vec{a}_2) \sim 2DL^2|\sin\gamma| \tag{30}$$

where $\sim$ denotes an asymptotic relationship (only giving the leading term). With the help of equations (26), (30) and (21) we find

$$\begin{aligned} B_2^{iso} &= -\frac{1}{2}\int -2DL^2|\sin\gamma|\frac{1}{4\pi}\cdot\frac{1}{4\pi}d\Omega 1 d\Omega_2 \\ &= \frac{\pi}{4}DL^2 \end{aligned} \tag{31}$$

It is this (excluded) volume which determines when the rods are strongly interacting, rather than the proper volume of the rod, being $v_0 = (\pi/4)D^2L$. This will be the case when the number density of rods reaches the order of 1 rod per v_{excl}, i.e. $B_2^{iso}\rho = O(1)$.

The next step would be to determine B_3. While the evaluation of the second virial coefficient B_2 proved perfectly feasible, the third virial coefficient B_3 requires extensive numerical calculation because it involves all possible relative orientations of triplets of particles. Fortunately it can be shown that for thin long rods B_3 makes a negligible contribution to the free energy (and hence to the derived thermodynamic functions such as chemical potential and pressure). To see how this comes about we write the free energy in the isotropic phase in terms of the combination $B_2^{iso}\rho$ (which will be of order 1 near the phase transition)

$$\frac{F^{iso}}{NkT} = constant + \ln\rho + B_2^{iso}\rho + \frac{B_3^{iso}}{2(B_2^{iso})2}(B_2^{iso}\rho)^2 + \ldots \tag{32}$$

We see that the relative importance of the third virial contribution is determined by the ratio $(B_3^{iso}/(B_2^{iso})^2)$. When we look at equation (24) we see

that to obtain the third virial coefficient we can start from a configuration in which two rods overlap (this gives a contribution of $O(L^2D)$, just like the second virial coefficient) and subsequently put the third rod in the overlap area of the first two rods. If the three rods are not coplanar the centre point of the third rod probes a volume of $O(LD^2)$ and this leads to a contribution to B_3 of order L^3D^3. Onsager gave some further geometric arguments to estimate the relative contribution of the (nearly) coplanar configurations and put forward the following scaling behaviour

$$\frac{B_3^{iso}}{(B_2^{iso})2} \sim \frac{D}{L}(\ln\frac{l}{D} + const) \tag{33}$$

which means it is small in the limit of thin rods ($L >> D$). Recently Frenkel [48] evaluated B_3, by means of Monte Carlo simulations. From his results it follows that the ratio $(B_3^{iso}/(B_2^{iso})^2)$ asymptotically indeed obeys the scaling relation (33) but the limit where the third virial contribution may be neglected is only reached for very high L/D.

In the nematic phase the domination of the second virial contribution is not obvious. In the extreme case of perfectly parallel (sphero)cylinders v_{excl} is no longer much larger than v_0 and B_3 scales like v_0^2. In this case the relative importance of B_3 (and the higher virial coefficients) is much more like the case of spheres and may never be neglected. The crucial question now is whether the clusters in the nematic phase are similar to those in the isotropic phase or to those in the perfectly aligned state. Luckily we shall see that at the isotropic-nematic phase transition the order is moderately high but independent of L/D. Thus by making L/D so large that all typical angles are much larger than D/L, we can be confident higher virial coefficients may be neglected. This point makes Onsager's (second virial) theory an exact theory for L/D$\rightarrow \infty$.

We will now consider the isotropic-nematic transition assuming that the expansion can be limited to the B_2 term. Introducing the dimensionless concentration

$$c \equiv (B_2^{iso}\rho) = \frac{\pi}{4}L^2D\frac{N}{V} = \frac{L}{D}v_0\frac{N}{V} = \frac{L}{D}\phi \tag{34}$$

where ϕ is the volume fraction of rods, we can write the free energy in the form

$$\frac{F[f]}{NkT} \cong constant + \ln c + \sigma[f] + c\rho[f] \tag{35}$$

where $\sigma[f]$ is related to the orientational entropy as given in equation (22) and the contribution $c\rho[f]$ is also entropic in nature

$$\rho[f] \equiv \frac{4}{\pi}\int |\sin\gamma(\vec{a}_1,\vec{a}_2)| f(\vec{a}_1)f(\vec{a}_2)d\Omega_1 d\Omega_2 \tag{36}$$

The isotropic-nematic transition originates from a competition between these two types of entropy: for low concentrations the orientational entropy dominates and is maximized by an isotropic distribution, whereas for high concentrations the excluded-volume term becomes more important which favours a nematic distribution. In the isotropic phase the orientation distribution function is given by eq. (21) which immediately leads to

$$\sigma_{iso} = 0 \qquad \rho_{iso} = 1 \tag{37}$$

and therefore the free energy in the isotropic phase takes the form

$$\frac{F^{iso}}{NkT} = constant + \ln c + c \tag{38}$$

To treat the nematic phase we must first minimize the free energy with respect to the orientation distribution function f. This can be done formally considering F as a functional of f while taking into account the normalization condition (20) by subtracting $\lambda' \int f(\vec{a}) d\Omega$ (λ' being a Lagrange undetermined multiplier) and then minimizing the resulting expression. This means the functional derivative must be 0 or

$$\frac{\partial}{\partial f}\left(\frac{F[f]}{NkT}\right) = \lambda' \tag{39}$$

An alternative route is to choose a (normalized) trial function with one or more variational parameters and then minimize the free energy with respect to these parameters. For illustrative purposes we shall use a Gaussian distribution function [49] here

$$\begin{aligned} f(\theta) &\sim \frac{\alpha}{4\pi}\exp(-\frac{1}{2}\alpha\theta^2) \qquad 0 \le \theta \le \frac{\pi}{2} \\ &\sim \frac{\alpha}{4\pi}\exp(-\frac{1}{2}\alpha(\pi-\theta)^2) \quad \frac{\pi}{2} \le \theta \le \pi \end{aligned} \tag{40}$$

This function only depends on the polar angle θ because of the uniaxial symmetry of a nematic phase. Using the Gaussian distribution one obtains to leading order (large α)

$$\sigma(\alpha) \sim \ln(\alpha) - 1 \tag{41}$$

$$\rho(\alpha) \sim \frac{4}{\sqrt{\pi\alpha}} \tag{42}$$

Substituting these results in equation (35) yields the following expression for F valid for large α

$$\frac{F(\alpha)}{NkT} \sim constant + \ln c + \ln\alpha - 1 + \frac{4c}{\sqrt{\pi\alpha}} \tag{43}$$

Minimizing this expression with respect to α leads to

$$\alpha \sim \frac{4c^2}{\pi} \tag{44}$$

and thus

$$\frac{F^{nem}}{NkT} \sim constant + 3\ln c + \ln\left(\frac{4}{\pi}\right) + 1 \tag{45}$$

The treatment given above is only valid for α sufficiently large, say $\alpha \geq 10$.

Comparing the free energies of the isotropic and nematic phase we note that F^{nem} becomes smaller than F^{iso} for $c > 4.03$ which indicates the possibility of a phase transition. To be in mechanical and chemical equilibrium the isotropic and nematic phase must have the same osmotic pressure and the same chemical potential

$$\Pi^{iso}(c_i) = \Pi^{nem}(c_n) \qquad \mu^{iso}(c_i) = \mu^{nem}(c_n) \tag{46}$$

which determine the concentrations in the isotropic and nematic phase, c_i and c_n. From the thermodynamic relations

$$\Pi = -(\partial F/\partial V)_{N,T} \qquad \mu = (\partial F/\partial N)_{V,T} \tag{47}$$

one obtains - using the free energy expressions (38) and (45) for the isotropic and nematic phase - the following coexistence conditions:

$$\begin{aligned} c_i(1+c_i) &= 3c_n \\ \ln c_i + 2c_i &= 3\ln c_n + \ln\frac{4}{\pi} + 3 \end{aligned} \tag{48}$$

From this we find the following coexisting concentrations

$$c_i = 3.45 \qquad c_n = 5.12 \tag{49}$$

implying (via equation (44))

$$\alpha = 33.4 \tag{50}$$

which is reasonably large (thus justifying the use of the Gaussian trial function). Finally, the usual measure of the ordering in the nematic phase is the nematic order parameter given by

$$S = < P_2(\cos\theta) > = \left\langle \frac{3}{2}\cos^2\theta - \frac{1}{2} \right\rangle \sim \left\langle 1 - \frac{3}{2}\theta^2 \right\rangle \sim 1 - \frac{3}{\alpha} = 0.910 \tag{51}$$

Here we have used that for a Gaussian distribution function asymptotically

$$< \theta^2 > \sim \frac{2}{\alpha} \tag{52}$$

The accuracy of the results obtained here with the Gaussian distribution function can be assessed by comparing them with the values obtained by an accurate numerical calculation [50]

$$c_i = 3.290 \qquad c_n = 4.191 \qquad S = 0.7922 \tag{53}$$

Onsager's (second virial) theory of the isotropic-nematic transition is accurate for $L/D >> 1$ (and in fact it is an exact theory for $L/D \rightarrow \infty$). The question then arises "how long should the rods be for the theory to have quantitative validity?" In order to quantify the necessary length Straley [51] considered the first correction term (the third virial contribution) to the Onsager theory. Straley estimates that up to $L/D \cong 20$ the contribution of the third virial term to the free energy (evaluated at the transition density) is at least comparable to the contribution of the second virial term. For L/D values as high as 100 he finds that the contribution of the third virial term is still about 10% of the second term. Using simulation results for the higher virial coefficients of hard spherocylinders [48] it turns out that Straley's estimate is remarkably accurate for $L/D = 100$ but that for the lower L/D values he is slightly too pessimistic about the quantitative accuracy of the Onsager theory. For example for $L/D = 10$ the contribution of the third virial term is certainly not more than 50% of that of the second virial term. Furthermore simulation results indicate that - whereas the contribution of B_3 remains substantial up to $L/D \cong 10^2$- the contributions of the higher virial terms decrease very quickly with increasing elongation. This means that for intermediate elongations the incorporation of the third virial contribution in the Onsager theory of the isotropic-nematic phase transition suffices to make the theory quantitatively accurate. Recent calculations by Tjipto-Margo and Evans [52] show that this is indeed the case for length-to-breadth ratios of 10 while even for length-to-breadth ratios as small as 5 incorporation of the third virial contribution leads to results that lie only about 10% above Monte Carlo results.

For elongations below five the second and third virial terms do not suffice to make the theory for the isotropic-nematic phase transition quantitatively accurate. In fact it may be surmised that all higher virial coefficients have to be somehow incorporated in the theory. Unfortunately at the present time the statistical mechanics of fluids of rodlike particles is not sufficiently well developed to provide confident answers on how to do this. Nevertheless a number of interesting attempts have been made to incorporate the higher virial coefficients, which we recently reviewed [53].

5. Onsager Theory for Bidisperse Systems

5.1. STARTING EQUATIONS

Another factor which is of importance for the interpretation of experimental results, is the influence of polydispersity. Even when prepared with great care synthetic colloids tend to be somewhat polydisperse. This may have important consequences for the phase behaviour. For example bidisperse solutions of rod-like particles show new and interesting phase behaviour such as triphasic isotropic-nematic-nematic equilibria. Our discussion of isotropic-nematic and nematic-nematic phase equilibria and the triphasic isotropic-nematic-nematic equilibrium in bidisperse rodlike systems is entirely based upon equations derived in the paper by Odijk and Lekkerkerker [54]. We will not repeat the derivation of these equations in detail but summarize the pertinent equations in this section and discuss them along the way. To facilitate comparison with ref. [54] we adhere to its notation as much as possible.

We start with a solution of hard rods with the same diameter D but two different lengths L_j ($j = 1, 2$; for sake of definiteness we denote the longer rods by subscript 2). The volume of the system is V, the number of short and long rods N_1 and N_2. Onsager [3] described the nematic phase of a dilute solution of long rods in terms of function $f_j(\theta)$ which describes the distribution of angles θ of the rods of type j around the director. The occurrence of an isotropic state (with f_j constant) or a nematic state (with a peaked distribution) is caused by a competition between orientational entropy and translational entropy. Onsager defined σ_j as a measure for the orientational entropy

$$\sigma_j \equiv \int f_j(\theta) \ln[4\pi f_j(\theta)] d\Omega \tag{54}$$

which acquires its minimum value of 0 in the isotropic state but increases as the orientational entropy decreases. $d\Omega$ indicates integration over all angles. The relevant part of the translational entropy derives from the two-particle interaction in the form of the excluded volume between two hard rods (with length L_j and L_k) which depends on their mutual angle γ

$$v_{excl} \sim 2DL_jL_k|\sin\gamma| \tag{55}$$

A measure for the average excluded volume interaction between rods of type j and k is given by the average of its angular dependence

$$\rho_{jk} \equiv \frac{4}{\pi}\int\int |\sin\gamma| f_j(\theta) f_k(\theta') d\Omega d\Omega' \tag{56}$$

which is 1 in the isotropic state and more favorable (between 0 and 1) in the nematic state. The total free energy F of the bidisperse system may be written in terms of these parameters as

$$\frac{F}{(N_1+N_2)kT} \cong constant + \ln c + (1-x)\ln(1-x) + x\ln x + \qquad (57)$$
$$(1-x)\sigma_1 + x\sigma_2 + c[(1-x)^2\rho_{11} + 2x(1-x)q\rho_{12} + x^2q^2\rho_{22}]$$

where k and T have their usual meaning of Boltzmann's constant and absolute temperature. In this equation $x \equiv N_2/(N_1+N_2)$ is the mole fraction of the longer rods and c is the total number density of rods rendered dimensionless by relating it to the excluded volume v_{excl} between two randomly oriented short rods

$$c \equiv v_{excl}\frac{N_1+N_2}{V} \equiv \frac{\pi}{4}L_1^2 D\frac{N_1+N_2}{V} \qquad (58)$$

Since c is related to the excluded volume of two short rods, the excluded volume terms in eq. (57) which involve one or two longer rods are multiplied by q or q^2, with

$$q \equiv L_2/L_1 \qquad (59)$$

Once expression (57) for the free energy is known, we must minimize it with respect to the orientational distribution at a given c and x. One way of doing this is using a trial function with one or more variational parameters. A convenient choice for the angular distribution of rod j in the nematic state is the Gaussian trial function [49]

$$\begin{aligned} f(\theta) &\equiv \frac{\alpha_j}{4\pi}\exp(-\frac{1}{2}\alpha_j\theta^2) \qquad 0 \le \theta \le \frac{\pi}{2} \qquad (60)\\ &\equiv \frac{\alpha_j}{4\pi}\exp(-\frac{1}{2}\alpha_j(\pi-\theta)^2) \quad \frac{\pi}{2} \le \theta \le \pi \end{aligned}$$

which gives good qualitative results for the isotropic-nematic phase transition for monodisperse rods and is getting more accurate as the phase is more highly ordered. α_j is the variational parameter of this trial function. To determine its value we must know the expressions for σ_j and ρ_{jk} obtained by substituting eq. (60) in eqs. (54) and (56):

$$\sigma_j \sim \ln\alpha_j - 1 \qquad (61)$$

$$\rho_{jk} \sim \frac{4(\alpha_j+\alpha_k)^{1/2}}{(2\pi)^{1/2}\alpha_j^{1/2}\alpha_k^{1/2}} \qquad (62)$$

which are the first terms of asymptotic expansions valid for large α_j. Using these expressions in eq. (57) and minimizing with respect to α_1 gives us

$$\frac{1}{2}\pi^{1/2}c^{-1}\alpha_1^{1/2} = (1-x) + 2^{1/2}xqh(Q) \tag{63}$$

with definitions

$$Q \equiv \alpha_2/\alpha_1 \tag{64}$$

$$h(Q) \equiv Q^{1/2}g(Q) \equiv \left(\frac{Q}{Q+1}\right)^{1/2} \tag{65}$$

A similar equation as (63) is acquired upon minimizing F with respect to α_2; both equations may be combined to obtain an expression only involving the ratio of both α s

$$Q^{1/2} = \frac{q[xq + 2^{1/2}g(Q)(1-x)]}{[2^{1/2}h(Q)xq + (1-x)]} \tag{66}$$

This is an implicit equation for Q and although we cannot obtain an explicit form for Q, its value is easily found by iteration. Note that this equation only contains the mole fraction x and not the concentration c , which implies Q = Q(x). Since this in turn implies that the right-hand side of eq. (63) only depends on x, we find that the concentration dependence of the α's remains quadratic like in the monodisperse case, cf. equation (44).

To locate phase transitions we must know the osmotic pressure and chemical potential of both types of rods. These are calculated as derivatives of the free energy (57). In the isotropic phase (denoted by subscripts i) we get in dimensionless notation

$$\tilde{\Pi}_i \equiv -\frac{v_{excl}}{kT}\left(\frac{\partial F}{\partial V}\right)_{N_1,N_2,T} = c_i + c_i^2[(1-x_i)^2 + 2x_i(1-x_i)q + x_i^2q^2] \tag{67}$$

$$\tilde{\mu}_{1i} \equiv \frac{1}{kT}\left(\frac{\partial F}{\partial N_1}\right)_{N_2,V,T} = \ln c_i + \ln(1-x_i) + 2c_i[(1-x_i) + x_iq] \tag{68}$$

$$\tilde{\mu}_{2i} \equiv \frac{1}{kT}\left(\frac{\partial F}{\partial N_2}\right)_{N_1,V,T} = \ln c_i + \ln x_i + 2c_i[(1-x_i)q + x_iq^2] \tag{69}$$

where the isotropic values $\sigma_j = 0$ and $\rho_{jk} = 1$ have been used. In the nematic state (denoted by subscripts a) matters are more complicated because of expressions (61) and (62) for σ_j and ρ_{jk}. By elaborate rearrangements [54] the excluded volume term (in square brackets) in eq. (57) could be shown equal to 2 in the Gaussian approximation, which results in

simple expressions

$$\tilde{\Pi}_a \sim 3c_a \tag{70}$$

$$\tilde{\mu}_{1a} \sim 3\ln c_a + \ln\frac{4}{\pi} + 3 + \xi'(x_a) \tag{71}$$

$$\tilde{\mu}_{2a} \sim 3\ln c_a + \ln\frac{4}{\pi} + 3 + \xi"(x_a) \tag{72}$$

The most remarkable fact of these equations is that the osmotic pressure only depends on the total number density of rods and not on the mole fraction. The mole fraction dependence of each chemical potential is restricted to one term, which does not depend on the concentration

$$\xi'(x_a) \equiv \ln(1-x_a) + 2\ln(1-x_a+2^{1/2}x_a q h) - \frac{2^{3/2}(Q-1)x_a g}{[2^{1/2}(1-x_a)g + x_a q]} \tag{73}$$

$$\xi"(x_a) \equiv \ln x_a + 2\ln\{q[2^{1/2}(1-x_a)g + x_a q]\} + \frac{2^{3/2}(Q-1)(1-x_a)g}{[2^{1/2}(1-x_a)g + x_a q]} \tag{74}$$

By equating the osmotic pressure and chemical potentials in the isotropic and nematic phases, Odijk and Lekkerkerker [54] were able to construct a fair part of the phase diagram including a reentrant phase. However, they did not notice the existence of a nematic-nematic phase transition and the corresponding isotropic-nematic-nematic triple point which we will discuss in the next sections.

5.2. COEXISTENCE BETWEEN TWO NEMATIC PHASES

When we study the possible coexistence between two nematic phases, we must realize that the osmotic pressure and chemical potentials are given by the same expressions in both phases. To obtain two different nematic phases there must be two states, denoted by I and II , with *different* c_a and/or x_a having the *same* osmotic pressure and chemical potentials. When we look at eq.(70) we notice that equality of osmotic pressure requires equality of total number density of rods:

$$c_{aI} = c_{aII} \tag{75}$$

When we use this knowledge in equations (71) and (72), they reduce to

$$\xi'(x_{aI}) = \xi'(x_{aII}) \tag{76}$$

and

$$\xi"(x_{aI}) = \xi"(x_{aII}) \tag{77}$$

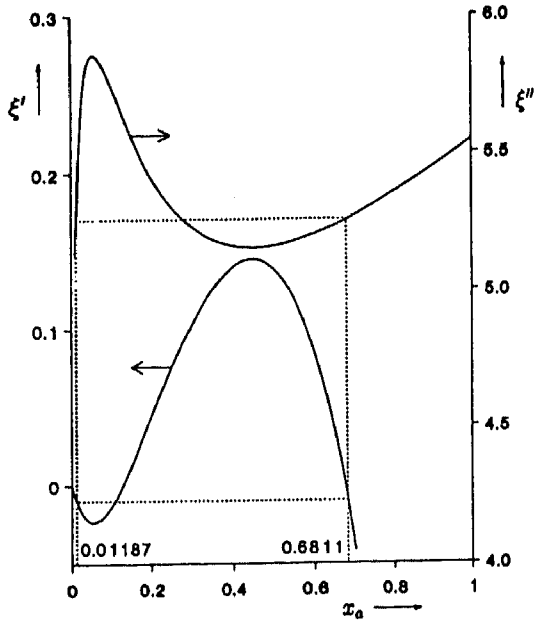

Figure 7. The mole fraction dependent parts of the chemical potentials of short and long rods for $q = 4$. The dashed lines indicate the coexistence of $x_{aI} = 0.01187$ and $x_{aII} = 0.6811$, at which compositions both chemical potentials are equal.

Thus the question of coexistence of two nematic phases is now reduced to the behaviour of ξ' and ξ" as a function of x_a.

In figure 7 we give ξ' and ξ" for $q = 4$. Both functions are non-monotonous so it is possible for two different x_a values to have the same value of ξ' and/or ξ" . The minimum of ξ' is located at the same x_a as the maximum of ξ" and vice versa. This is a manifestation of the Gibbs-Duhem relation

$$(1 - x_2)\left(\frac{\partial \mu_1}{\partial x_2}\right)_{\Pi,T} + x_2\left(\frac{\partial \mu_2}{\partial x_2}\right)_{\Pi,T} = 0 \qquad (78)$$

which in the present case may be rewritten as

$$(1 - x_a)\left(\frac{\partial \xi'}{\partial x_a}\right)_{c_a,T} + x_a\left(\frac{\partial \xi"}{\partial x_a}\right)_{c_a,T} = 0 \qquad (79)$$

from which the relation between the extrema of ξ' and ξ" is obvious. In the

TABLE 1. Mole fractions and Q, ξ' and ξ'' values at the nematic-nematic phase transition for different length ratios q

q	x_{aI}	x_{aII}	Q_I	Q_{II}	ξ'	ξ"
3.2	0.1438	0.3080	4.617	5.067	-0.0566	4.134
3.3	0.08739	0.4079	4.603	5.548	-0.0455	4.300
3.5	0.04432	0.5236	4.746	6.369	-0.0295	4.605
4	0.01187	0.6811	5.301	8.407	-0.0101	5.257
5	0.00119	0.8205	6.615	13.05	-0.00115	6.268

region in between the extrema the system is unstable; here we can show

$$\left(\frac{\partial \mu_2}{\partial x}\right)_{\frac{N_1+N_2}{V},T} < 0 \tag{80}$$

from which it is clear that the system will spontaneously demix in this region. The extrema delimiting this region are the spinodal points. The dashed line in figure 7 connects the coexisting compositions for which both ξ' and ξ" are equal. In the intermediate region phase separation will occur. In table 1 we give the nematic-nematic phase transition for various length ratios.

In figure 8 we give some curves for ξ' for different values of q (as we have seen above, the curves for ξ" offer the same information). We see that the extrema are getting less pronounced and shift towards each other for lower q values. At $q = 3.1672$ they vanish and thus below this value a nematic-nematic phase transition ceases to exist.

Finally, we want to stress that the coexistence relations discussed above are fulfilled irrespective of the concentration c_a . However, an important point we did not address is the stability of the nematic phases compared to the isotropic phase. This will be considered in the next section.

5.3. PHASE EQUILIBRIA INVOLVING THE ISOTROPIC PHASE

Up to now we did not take the isotropic phase into consideration. For high concentrations the free energy of this phase is dominated by the last term in eq.(57), which increases linearly with the concentration (remember that $\rho_{jk} = 1$ in the isotropic phase). The same term for the nematic phase is constant since in that case $\rho_{jk} \propto c^{-1}$ (as follows from eq.(62) and the discussion following eq.(66)). Therefore, at high concentrations, the free energy of the isotropic phase will be higher than for the nematic phase and the isotropic phase will not interfere with the nematic-nematic phase equilibrium discussed in the preceding section.

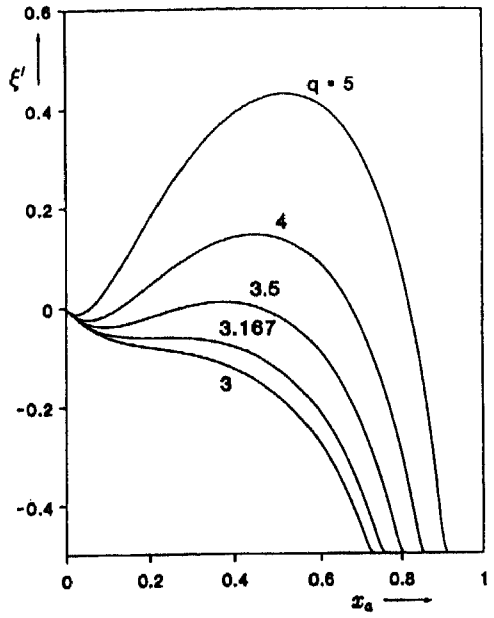

Figure 8. The mole fraction dependent part, ξ', of chemical potential μ_1 for different values of q. At $q = 3.167$ the extrema merge to an inflection point, so that below this q value the chemical potential is decreasing monotonously and no nematic-nematic transition is possible.

Of course, at very low concentrations the isotropic phase is the stable state so there should be a point where the three phases are in equilibrium. This point is found by equating the osmotic pressure and chemical potentials found for the nematic-nematic equilibrium to those of the isotropic state. As will become evident later on, we may use the simplified forms valid for $x_i q << 1$ [54] in the isotropic phase. Under this assumption equating eqs.(67) and (70) gives

$$c_i + c_i^2 = 3c_a \tag{81}$$

while equating the difference between eqs. (69) and (68) to the difference between (72) and (71) gives

$$\ln x_i + 2c_i(q-1) = \xi"(x_a) - \xi'(x_a) \tag{82}$$

Finally equating eqs. (68) and (71) and eliminating c_a by means of eq. (81) leads to

$$\ln c_i + 2c_i = 3\ln\frac{c_i + c_i^2}{3} + \ln\frac{4}{\pi} + 3 + \xi'(x_a) \tag{83}$$

TABLE 2. Concentrations and mole fractions at the isotropic-nematic-nematic triple point for different length ratios q

q	c_i	x_i	$c_{aI} = c_{aII}$	x_{aI}	x_{aII}
3.2	3.375	$2.35\ 10^{-5}$	4.921	0.1438	0.3080
3.3	3.390	$1.30\ 10^{-5}$	4.960	0.08739	0.4079
3.5	3.412	$4.02\ 10^{-6}$	5.017	0.04432	0.5236
4	3.438	$2.13\ 10^{-7}$	5.086	0.01187	0.6811
5	3.450	$5.4\ 10^{-10}$	5.118	0.001188	0.8205

Now solution of these equations is simple: $\xi'(x_a)$ is known from the previous paragraph, so eq. (83) only contains c_i as an unknown variable, which may be solved iteratively. Then x_i is found from (82) and c_a is found from (81). The result for different q values is given in table 2. From the very small x_i values it is clear that indeed $x_i q << 1$ so that the use of the simplified forms of the coexistence equations is entirely justified.

For lower concentrations a simple isotropic-nematic equilibrium is found by solving the three equations (81-83) for three unknown variables, eg. c_i , c_a and x_a. This is done for different values of the fourth variable x_i , which may be chosen freely.

5.4. GRAPHIC REPRESENTATION OF THE PHASE DIAGRAMS

To present a graphic illustration of the results obtained for $q = 3.5$, we give a $\tilde{\Pi} - x$ diagram in figure 9 and a diagram in terms of volume fractions in figure 10. The volume fraction representation may be more convenient from an experimental standpoint. The volume fractions are obtained straightforwardly from the definition of x ($\equiv N_2/(N_1 + N_2)$) and c (eq.(58))

$$\phi_1 = \frac{\pi}{4} L_1 D^2 \frac{N_1}{V} = \frac{D}{L_1}(1-x)c \tag{84}$$

$$\phi_2 = \frac{\pi}{4} L_2 D^2 \frac{N_2}{V} = \frac{D}{L_1} xqc \tag{85}$$

Note that the three coexisting phases that lie on a triple line in the field-density presentation of figure 9, form a three-phase triangle in the density-density representation of figure 10. As we have seen the mole fractions of the coexisting nematic phases are independent of concentration, which results in vertical phase boundaries in figure 9 and corresponding straight lines in figure 10. The tie lines which are horizontal lines in figure 9 because of equality of osmotic pressure, are denoted in figure 10 by sloping lines.

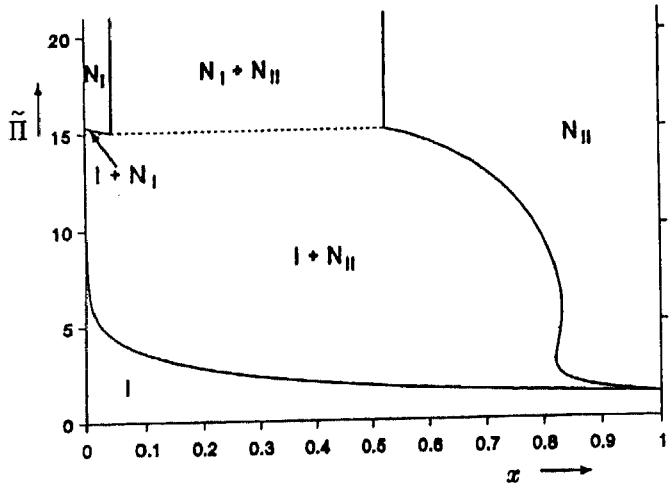

Figure 9. A $\tilde{\Pi} - x$ diagram for $q = 3.5$. The dashed line is the triple line, where an isotropic (I) and two nematic (N_I and N_{II}) phases coexist. In case $x_i q$ not $<< 1$ the full Gaussian expressions for μ_1, μ_2 and Π were solved iteratively. Note the re-entrant phenomenon [54] near $x_a = 0.82$.

In a volume fraction representation these tie lines may be shown to form straight lines [55].

For comparison we give in figure 11 a phase diagram for q=2.5 which is below the critical length ratio of 3.167. This diagram only shows a simple isotropic-nematic transition.

Lines A, B and C in figures 10 and 11 are lines of increasing $\tilde{\phi}^{tot}$ $(= \tilde{\phi}_1 + \tilde{\phi}_2)$ for the dispersion as a whole, for different ϕ_1/ϕ_2 ratios. Experimentally, these lines represent the phase behaviour upon evaporating the solvent from the bidisperse mixture. For each of these lines, the volume fractions of the coexisting isotropic and anisotropic phases $(\tilde{\phi}^{i,a} = (\tilde{\phi}_1 + \tilde{\phi}_2)^{i,a})$ are determined from the tie lines as a function of $\tilde{\phi}^{tot}$, as represented in the upper plots in figure 12A, B (q=3.5) and figure 13A-C (q=2.5). In the lower plots of figures 12 and 13, V^α/V^{tot} indicates which fraction of the total volume of the system is occupied by phase α. These representations will later be used for comparison with experimental results (in section 6.4)

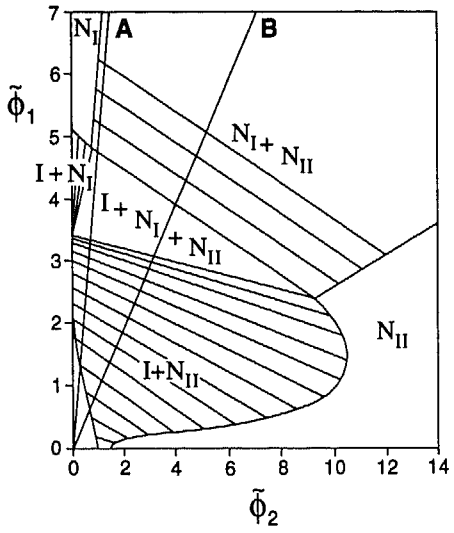

Figure 10. A phase diagram for $q = 3.5$ in terms of volume fractions $\tilde{\phi}_1 \equiv (L_1/D)\phi_1$ and $\tilde{\phi}_2 \equiv (L_1/D)\phi_2$. To avoid the need to fix aspect ratio L_1/D, both volume fractions were multiplied by this number. I, isotropic; N_I, N_{II} nematic. Coexisting phases in the biphasic region connected by tie lines. Lines A ($\phi_1/\phi_2 = 5$) and B ($\phi_1/\phi_2 = 1$) are profiles of increasing $\tilde{\phi}^{tot} \equiv \tilde{\phi}_1 + \tilde{\phi}_2$.

5.5. DISCUSSION

Our calculations based upon the Gaussian approximation, give a surprisingly simple picture of the nematic-nematic phase transition. Its origin is different from the isotropic-nematic transition, which is a result of a competition between orientational-entropy and excluded-volume terms in the free energy. In the Gaussian approximation the excluded-volume term in the nematic phase is independent of mole fraction and concentration. As a consequence excluded volume does not play a role in this phase transition and the transition must be explained solely from an intricate interplay between orientational entropy and entropy of mixing. Above q = 3.167 this leads to the existence of two nematic phases.

We wish to indicate that the present calculations are subject to some reservations. As shown in ref. [53], there exists an exact relationship between the orientational distribution functions of different rods in a polydisperse mixture, which is not fulfilled for Gaussian distribution functions. However, we wish to point out that the procedure of minimizing the free energy independently with respect to both distributions, makes the value for the free energy less sensitive to the precise form of the distribution functions. The

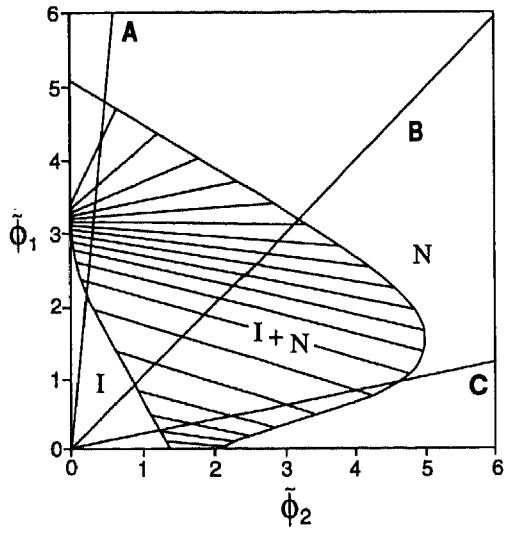

Figure 11. An analogous phase diagram as figure 10 without a triphasic region; here q = 2.5. Lines A ($\phi_1/\phi_2 = 10$), B($\phi_1/\phi_2 = 1$), and C($\phi_1/\phi_2 = 0.2$) are profiles of increasing $\tilde{\phi}^{tot}$.

fact that our calculation does not show a critical point which closes the nematic- nematic coexistence area in the phase diagram at higher concentrations may be due to this shortcoming. This behaviour was found both within the Flory theory [56] and in the series solution to the Onsager theory [57].

For comparison with experimental results the representation of figure 10 is most suitable. In this figure experiments which probe the phase behavior of bidisperse mixtures by adding or evaporating the solvent, will be represented by straight lines radiating from the origin. We see from the figure that even for a low length ratio of 3.5 a large range of compositions will pass through the three- phase area. Particularly, it appears that a very small mole fraction of long rods in the isotropic phase already leads to a three-phase equilibrium upon increase of the overall concentration. Further it is clear that -although the total number density of rods is the same in two coexisting nematic phases- the total volume fraction may be considerably different because of the difference in volume between the two kinds of rods.

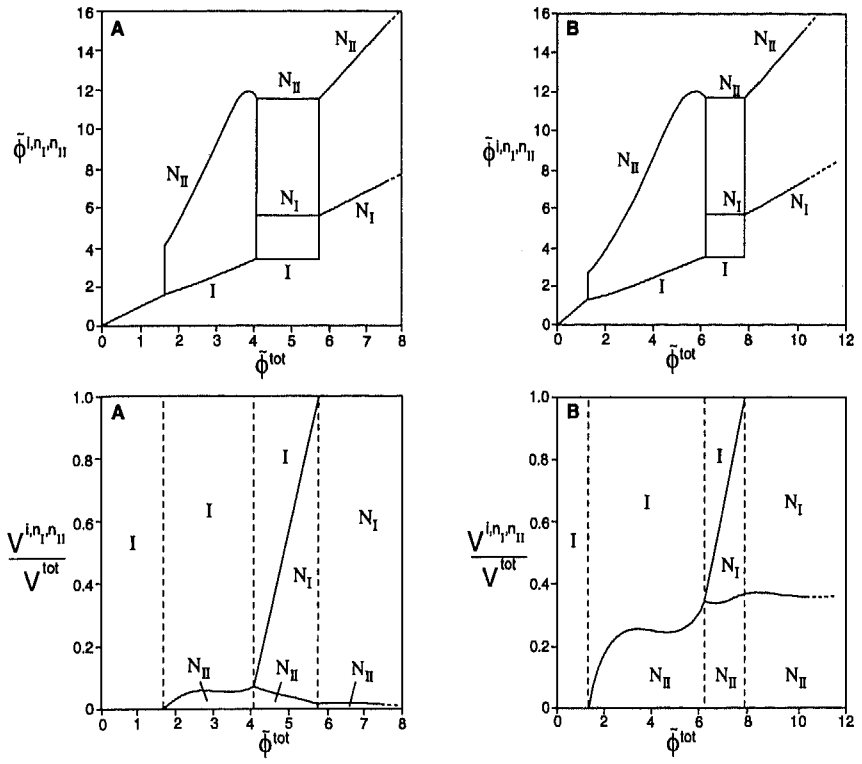

Figure 12. Upper plots: scaled volume fractions of coexisting isotropic and nematic phases in the system $L_2/L_1 = 3.5$, as constructed from the tie lines for profiles A and B in Figure 10. Lower plots: the relative amounts of isotropic and nematic phase for profiles A and B in Figure 10. (A) $\phi_1/\phi_2 = 5$; (B) $\phi_1/\phi_2 = 1$.

6. Experiments on the Isotropic-Nematic Phase Separation of a Dispersion of Organophilic Boehmite Rods

6.1. INTRODUCTION

We describe experiments on the isotropic-nematic phase transition in a dispersion of organophilic rodlike colloidal particles which can be modelled with a nearly hard particle interaction. The system studied is a dispersion of boehmite particles with an average length of about 200 nm and an aspect ratio of about 20, prepared according to a novel alkoxide route [42]. The boehmite core-particles were sterically stabilized by grafting a layer of poly(isobutene) on their surface [43].

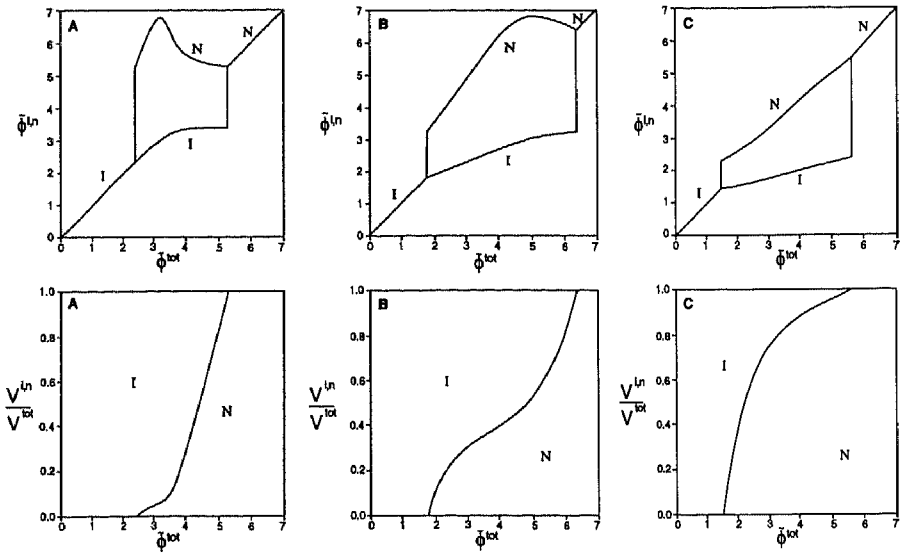

Figure 13. Upper plots: scaled volume fractions of coexisting isotropic and nematic phases in the system $L_2/L_1 = 2.5$, as constructed from the tie lines for concentration profiles A, B and C in Figure 11. Lower plots: the relative amounts of isotropic and nematic phase for profiles A, B and C in Figure 11. (A) $\phi_1/\phi_2 = 10$; (B) $\phi_1/\phi_2 = 1$; (C) $\phi_1/\phi_2 = 0.2$.

The boehmite dispersion studied here shows polydispersity in both the particle length and width. Nevertheless, the dispersion shows a fast isotropic-nematic phase transition above a certain critical volume fraction. To understand the effect of polydispersity, the coexisting concentrations are compared with those calculated with Onsager's theory extended to a (bidisperse) mixture of two particle lengths (see previous section). For bidisperse solutions, theory predicts the existence of a three-phase isotropic-nematic-nematic region. In the case of polydisperse rigid, nearly hard boehmite rods, a second nematic phase indeed emerged in the biphase dispersion, but not until after months of standing.

6.2. MATERIALS AND METHODS

The dispersion used (coded ASBIP10g) contains boehmite needles, about 200 nm long ($\sim$ 50% std.dev.), 10 nm wide ($\sim$ 25% std.dev.) and 8 nm thick, as determined by transmission electron microscopy. The aqueous dispersion of boehmite core particles was prepared hydrothermally (see ref. [42]).

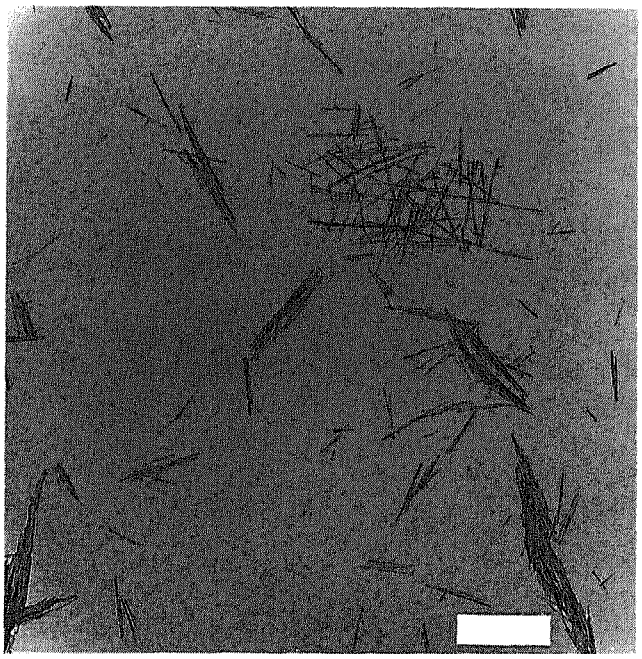

Figure 14. Transmission electron micrograph of ASBIP10g. The length of the bar represents $0.5\mu m$.

These particles were stabilized in cyclohexane by terminally grafting low molecular weight poly(isobutene) molecules on their surface, as described in ref. [43]. Based on the analogy with similar dispersions of spherical silica particles [58], we may assume that the grafted rods model a hard interaction. As a consequence of the larger boehmite concentration applied in the grafting procedure compared to that in ref. [58], the ASBIP10g dispersion contains a certain amount of clusters consisting of sideways aggregated needles. A transmission electron micrograph of the dispersion (figure 14) shows spindlelike bundles of clustered rods next to unclustered rods. It is yet uncertain whether the clusters are reversible aggregates or particle coagulates due to some stickiness of the rods.

Starting with a stock ASBIP10g dispersion of 7.36% w/v, the concentration was gradually increased by slowly blowing nitrogen through the dispersion under vigorous stirring. The lumps that form during concentration can easily be redispersed by stirring and sonication.

After phase separation, the weight concentration of the isotropic upper phase w^i was determined by pipetting off a known volume of upper phase, followed by drying and weighing. The weight concentration of the coexisting nematic lower phase w^n was determined from w^i, the total concentration

of the dispersion w and the volumes of the coexisting phases V^i and V^n, using

$$V^i w^i + V^n w^n = (V^i + V^n)w$$

Volume fractions were calculated from the expression $\phi^{i,n} = w^{i,n}/\rho_p$where ρ_p is the density of the organophilic boehmite particles ($\rho_p = 2.00 g cm^{-3}$).

The sample preparation for microscopic study was performed by depositing some dispersion (after being homogenized on a vortex stirrer) into the hollow of a glass slide, onto which a cover slip was put. Soon after preparation the dried dispersion at the borders of the cover slip prevents strong evaporation of the solvent. The sample was observed at a magnification up to 400x in a Zeiss Axioplan polarization microscope.

6.3. RESULTS

6.3.1. *Observations with the Naked Eye*

The initial ASBIP10g dispersion (7.36% w/v) appears quite translucent and shows birefringence when the sample tube is shaken. The relaxation time of this shear-induced birefringence is less than one second. On increasing the weight concentration above about 9.3% w/v, denoted by w_i (corresponding to a volume fraction of $\phi_i = 4.7$ vol.%) the dispersion starts to show turbidity, which disappears after shaking and reappears upon resting.

After standing one day, the turbid dispersion has separated into a dense phase on the bottom of the tube and a supernatant translucent colloidal dispersion. The lower phase is remarkably transparent and shows a fine structure of permanently birefringent domains, which gradually coarsens with time. The upper phase is isotropic, but already displays birefringence when the sample tube is only slightly moved. The interface between both phases is very sharp and moves easily under gravity, which can be observed by tilting the tube (see fig.15). After being at rest for about six months, a thin layer of newly formed birefringent phase was observed on top of the nematic phase. It appears that during this period the amount of lower nematic remains unchanged. So the new phase originated at expense of the isotropic upper phase. When the tube is tilted, the layer flows like the lower nematic phase and remains completely separated on top of it.

At a weight concentration of 35.9% w/v, denoted by $w_n(\phi_n = 18.0$ vol.%) the point is reached where the isotropic upper phase becomes unstable and the whole dispersion volume will be filled by the nematic phase. Above w_n, say at about 50% w/v ($\phi \approx 25$ vol.%), the monophasic nematic dispersion quite suddenly turns into a turbid, extremely viscous state. The particles appear completely immobilized in a glasslike state.

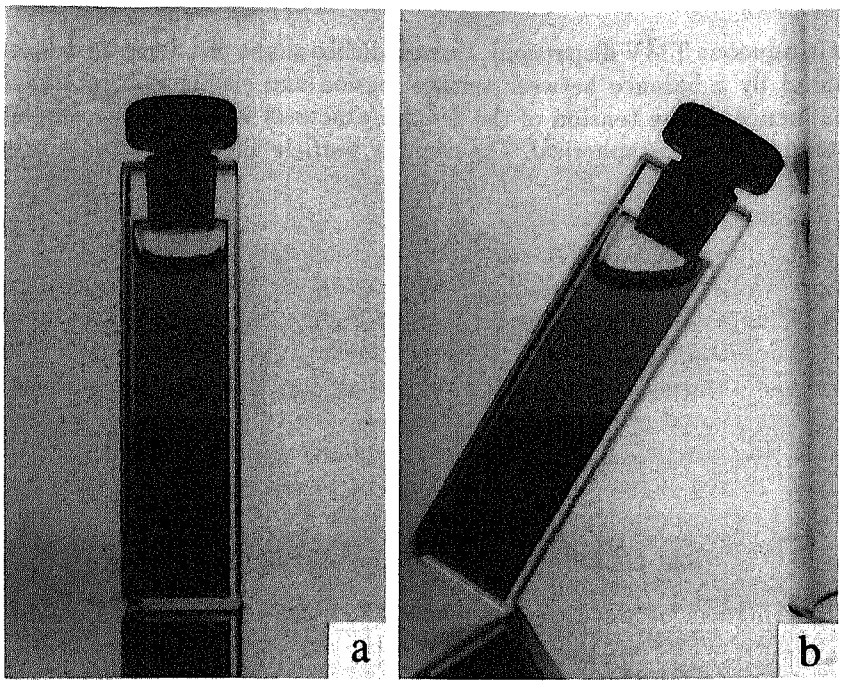

Figure 15. (a) Phase separation of ASBIP10g ($\sim$ 30% w/v); (b) 10 s after tilting the tube.

6.3.2. *Microscopic Observations*

The growth of the nematic phase follows different stages: In the first stage (A) there is the formation of small ($\sim 2 - 4\mu m$) birefringent elongated droplets (tactoids), which grow in the isotropic phase (atactosol), as shown in figure 16a. The large amount of droplets throughout the sample gives it visually a turbid appearance. After a few minutes (stage B), while the droplets are still nucleating, an irregularly structured continuous birefringent phase (tactosol) arises at the bottom of the sample (figure 16b). During the next few hours (stage C) the tactoids keep on growing until they are about $30\mu m$ in size (figure 16c). Some tactoids flow together (figure 16c, upper right part), and while they become larger, they sink under gravity and merge into the lower tactosol. Often, tactoids appear to nucleate and grow on the lower side of the glass coverslip. When such a tactoid has gained too much weight, a new droplet forms under the old one, connected to it by a thin "neck", recognized as a small dot in the tactoid. Then suddenly the lower tactoid separates from the upper one (the neck disappears and falls apart into small droplets) and starts to sink. The remaining part of the tactoid on the coverslip again grows and the whole process repeats itself.

As was indicated by Bernal and Fankuchen [23] by observation of tac-

toids in aqueous TMV dispersions, the spindlelike shape of a nematic droplet is caused by a balance between surface tension and elastic energy. Under the influence of the tension of the droplet/atactosol interface, the droplet will tend to become spherical. The nematic particle alignment counteracts the formation of a rounded surface by its elasticity. As a compromise, the droplets develop a spindle shape.

In the presence of air bubbles, the tactoids are lined up parallel to the air-sol interface. A special case is formed by domains of atactosol (atactoids), similarly spindle-shaped as the tactoids, surrounded by tactosol (figure 16c, lower right part). From the settling velocity and the optical contrast of the tactoids, it can be concluded that they have a markedly higher density and refractive index than the surrounding atactosol. During this tactoid growth, the structure of the underlying tactosol (as observed between crossed polars) coarsens and shows the beginning of a schlieren pattern. After one day of standing at rest (stage D) all tactoids have disappeared from the isotropic upper phase and the nematic lower phase exhibits a distinct schlieren texture (figure 16d): a pattern of threadlike brushes which extinguish between crossed polars. The brushes branch out from singular points, which are discontinuities in the mean alignment direction of the particles (referred to as the director). Around the singular points, the director changes continuously. As a consequence, when the object table is rotated, a singular point stays at a fixed position, while the dark brushes move around it. The schlieren texture resembles the defect structures observed in conventional thermotropic liquid crystals, and appears to be extremely sensitive to small disturbances. If the coverslip is shifted slightly, the whole texture changes immediately. The schlieren texture is distorted and new tactoids are being formed.

6.3.3. *Phase Diagram*

The experimentally determined boehmite volume fractions of the coexisting isotropic and nematic phases clearly depend on the total volume fraction (figure 17a). As a consequence, the amounts of nematic phase at several total volume fractions, shows a non-linear trend (figure 17b). For the monodisperse case, one would expect constant volume fractions and a linearly increasing amount of nematic phase in the biphasic region. It is expected that the experimentally found trends find their origin in the system's polydispersity, causing a fractionation effect in the rod-length distribution between the isotropic and anisotropic phases. However, visual inspection of the transmission electron micrographs taken of the isotropic and nematic phases which separated in the ASBIP10g dispersion (12.3% w/v) reveals no difference in average particle length or width.

Because theory is available for a bidisperse mixture of rod lengths (see

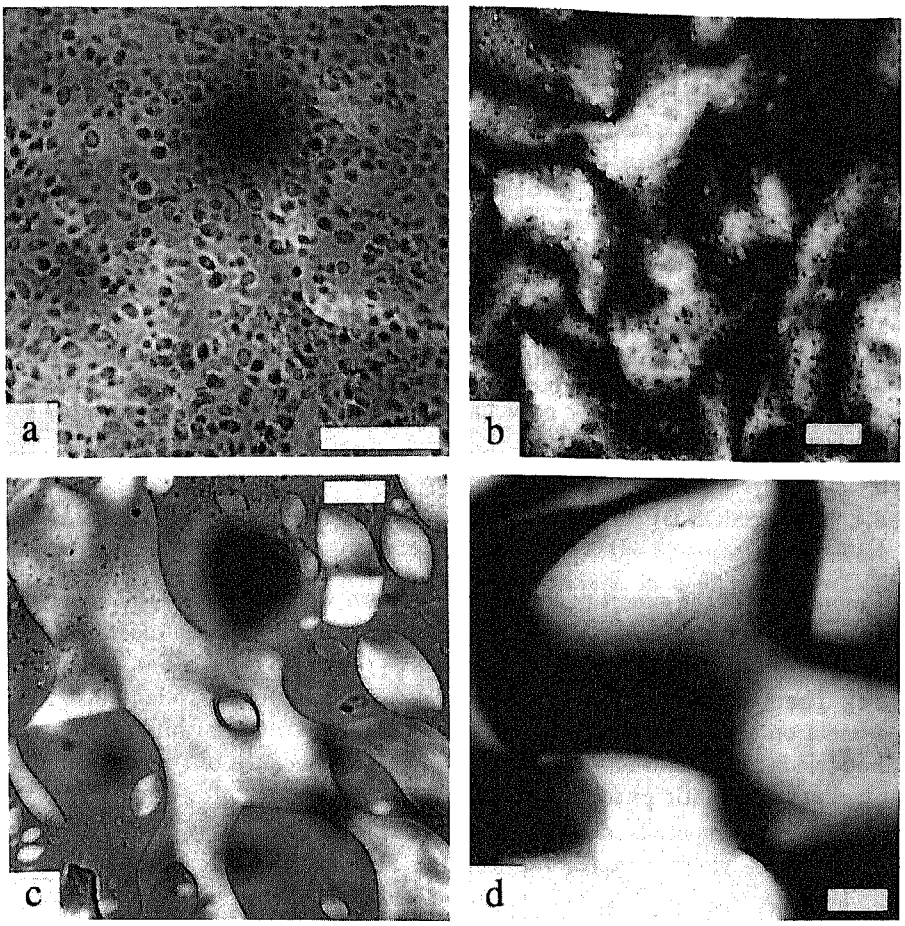

Figure 16. (a) Optical micrograph of the nucleation of very small nematic droplets (stage A). (b) Nematic droplets and underneath a continuous nematic lower phase with schlieren (stage B). (c) Grown-out tactoids (stage C). (d) Schlieren texture after completion of phase separation (stage D). All observations with crossed polars. The lengths of the bars represent $20\mu m$.

previous section), we will compare the trends in our experimental phase diagram for the polydisperse case with those in theoretical phase diagrams for the bidisperse case.

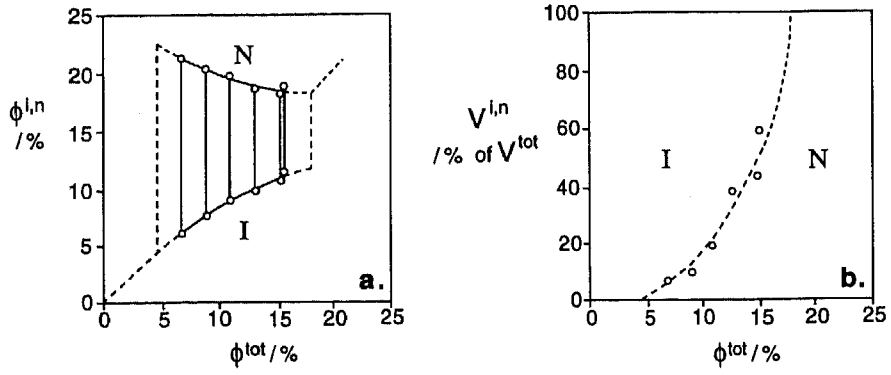

Figure 17. (a) Boehmite volume fractions of coexisting isotropic (I) and nematic (N) phases as a function of the total boehmite volume fraction, and the constructed phase diagram. (b) Volumes of nematic phase (in percentage of total dispersion volume) as a function of the total boehmite volume fraction.

6.4. DISCUSSION OF THE EXPERIMENTAL AND THEORETICAL PHASE DIAGRAMS

Comparison of the experimental phase diagram with the theoretical curves (figures 12 and 13), shows that the experimental findings agree most closely with the case of $L_2/L_1 = 2.5$ and a large ϕ_1/ϕ_2 ratio (the A-line in figure 11). The maximum in the $\tilde{\phi}^n$ versus $\tilde{\phi}_{tot}$ plot in figure 13 might also be present on the low volume fraction side of the experimental biphasic area, but this is difficult to investigate experimentally because of the very small amounts of nematic phase at that point.

The experimentally determined biphasic gap between $\phi_i = 4.7\%$ and $\phi_n = 18.0\%$ yields a ϕ_n/ϕ_i ratio of 3.8. For the monodisperse case one finds $\phi_n/\phi_i = 1.3$ (see section 4) so the widening of the biphasic gap due to polydispersity is evident. Case A in figure 11 is quite representative for our ASBIP10g system on choosing the following system parameters: 91% volume fraction of rods with length $L_1 = 200$nm (average rod length) and 9% volume fraction of rods with $L_2 = 500$nm (length of the few very long rods), both having D=10 nm. The above-mentioned experimental values of ϕ_i and ϕ_n are however lower than the values $\phi_i = 12\%$ ($\tilde{\phi}_i = 2.4$) and $\phi_n = 27\%$ ($\tilde{\phi}_n = 5.3$) predicted from figure 12A. Deviations from the theory are to be expected for the following reasons: (1) the particle aspect ratios in the ASBIP10g system are, strictly speaking, not large enough for the Onsager approach to be quantitatively valid; (2) the particle interaction might not be completely hard but may show some additional attraction or repulsion;

(3) because our system is polydisperse, its modeling by bidispersity might not fully explain the trends; and (4) the theory is based on the Gaussian approximation.

The experimentally found triphasic isotropic-nematic-nematic coexistence can be explained if we assume that the system shows a high enough polydispersity to reach a maximum L_2/L_1 ratio of about 3.5. As indicated in the introduction the formation of the second phase takes a considerable amount of time whereas the formation of the first nematic phase takes only about 1 day. The second nematic phase separates from the isotropic phase not until after months of standing. Guided by the theoretical phase diagrams presented in figure 12, the above experimental observations could be interpreted as the fast-formation of nematic phase N_{II} (high density, consisting mainly of the longer rods) and a metastable isotropic phase that slowly phase separates in a stable isotropic phase and nematic phase N_I (low density, consisting mainly of the shorter rods). Clearly considerable further experimental work has to be done to clarify the nature of the mechanism and properties of the isotropic-nematic-nematic phase separation.

6.5. CONCLUDING REMARKS

The results presented here are to our knowledge the first examples where the isotropic-nematic phase separation is observed in a dispersion which is a model for a hard rod system. In this system of sterically stabilized boehmite rods (on average 200 nm long, $L/D \approx 20$), the biphasic gap is situated between $\phi_i = 4.7\%$ and $\phi_n = 18.0\%$. At $\phi \approx 25\%$ the monophasic nematic transforms into an extremely viscous glass phase.

The nematic phase formation is initiated by the formation of small nematic droplets macroscopically, to be recognized as an increase in the turbidity of the dispersion. These tactoids slowly settle under gravity to form the continuous nematic phase. The effect of polydispersity on the phase diagram is, given the approximations, well predicted by the Onsager theory for bidisperse rod systems of large ϕ_1/ϕ_2 ratio. The three-phase isotropic-nematic-nematic equilibrium as predicted by theory is observed. The second nematic phase, which situates itself on top of the lower nematic phase, develops very slowly (period of months!). The reasons for this slow growth are still unclear at this moment.

7. Colloid-Polymer Mixtures: general formalism

7.1. INTRODUCTION

At the present time there is a growing interest in dispersions containing two "colloidal" components . These systems display new phenomena of fun-

damental interest and at the same time are of considerable technological importance. Of particular interest are the depletion interactions. This effective interaction is based on the exclusion of added polymer molecules from the region between two colloidal particles when their surface-surface separation becomes smaller than the diameter of the added polymer molecules. The resulting imbalance in osmotic pressure gives rise to an effective attraction between the colloidal particles [59,60,29]. This depletion force has been termed "attraction through repulsion" by Vrij.

We present a general formalism to treat these colloid-polymer mixtures. Subsequently, we use the formalism to study the influence of free, non-adsorbing polymer on the phase equilibria in dispersions of rodlike colloids (section 8). Finally, experimental results on the phase behaviour of dispersions containing sterically stabilized boehmite rods and polydimethylsiloxane/polystyrene are presented and compared with theoretical predictions (section 9).

7.2. FORMALISM

For the thermodynamic treatment of the phase separations that occur in colloid-polymer mixtures it is most convenient to consider the chemical potential μ_p of the polymer molecules as an independent thermodynamic variable [33]. This approach is different from the one adopted by other workers [31,32] in which polymer partitioning between the various phases is not taken into account. For this purpose we consider the osmotic equilibrium system illustrated in Fig. 18.

It consists of three compartments separated by two semi-permeable membranes, with solvent in I, polymer solution in II and a colloid-polymer dispersion in III. In the osmotic equilibrium system depicted in figure 18, the solvent, denoted by the subscript o, has a chemical potential μ_o throughout. In accordance with the practice in the rest of this paper, we will not mention the dependence on μ_o explicitly. Membrane II/III is permeable to polymer, denoted by the subscript p with concentration (number density) n_p^r in II and n_p in III. (The superscript r is used to indicate that we consider compartment II as the reservoir for the system of interest.) Finally the colloid denoted by the subscript C, has a concentration n_C in III. The osmotic pressure Π_p^r of the polymer solution in the reservoir is the pressure difference between II and I

$$\Pi_p^r = P_{II} - P_I \tag{86}$$

The osmotic pressure Π of the colloid-polymer mixture with respect to the solvent is the pressure difference between III and I

$$\Pi = P_{III} - P_I \tag{87}$$

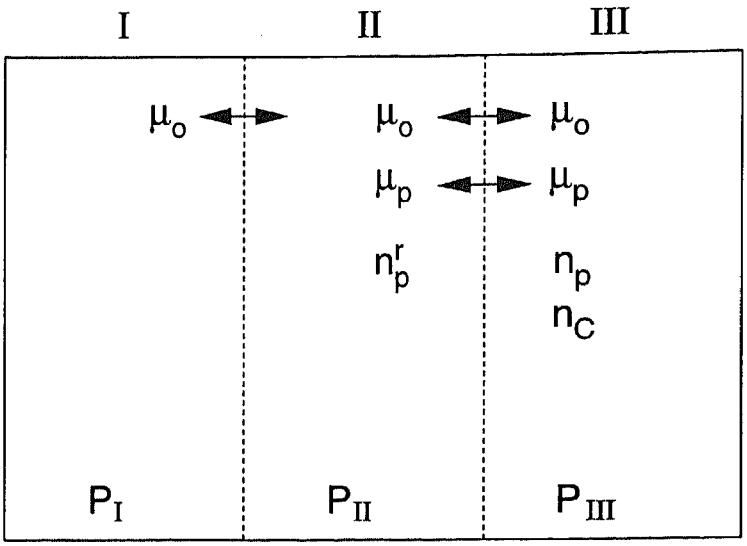

Figure 18. Osmotic equilibrium system consisting of three compartments separated by two semipermeable membranes, with solvent in I, polymer solution in II and a colloid-polymer dispersion in III. The solvent is denoted by the subscript o, the polymer by the subscript p and the colloid by the subscript C.

This osmotic pressure Π and the chemical potential μ_C of the colloidal component are now functions of the temperature T, the colloid concentration n_C and the chemical potentials μ_p of the polymer

$$\Pi = \Pi(n_C, T, \mu_p) \tag{88}$$

$$\mu_C = \mu_C(n_C, T, \mu_p) \tag{89}$$

To calculate these thermodynamic functions one has to start from a specific model for the system.

As a model for a colloid-polymer mixture we depict the colloidal particles as hard particles and the polymer molecules as interpenetrating spheres with diameter σ_p whose centers of mass cannot approach closer than a distance $\sigma_p/2$ from the surface of the colloidal particles. Consequently, around each colloidal particle there is a shell from which polymer molecules are effectively excluded.

The use of this model to describe colloidal dispersions containing non-adsorbing polymer was first suggested by Vrij [29]. In the theory of liquids this model is known as the "non- additive" hard sphere model and was used in the context of liquid-vapour transitions [61]. Here we show how it can be used in the study of the phase behaviour of colloid-polymer mixtures.

The appropriate thermodynamic potential to use here is the grand potential

$$\Omega = F - N_p \mu_p \tag{90}$$

which can be obtained from the grand canonical partition function

$$\Xi(N_C, \mu_p, V) = \sum_{N_p=0}^{\infty} z_p^{N_p} Z(N_C, N_p, V) \tag{91}$$

via the standard relationship

$$\Omega = -kT \ln \Xi \tag{92}$$

In eq. (91) z_p is the activity of the polymer molecules

$$z_p = \exp(\mu_p / kT) \tag{93}$$

For the evaluation of the grand canonical partition function we follow the line of thought used by Meijer and Frenkel [62] in a related problem. To begin with consider the case that we just have one polymer molecule in the colloidal dispersion. The (configurational part) of the canonical partition function of the system is then given by

$$Z(N_C, 1, V) = \frac{1}{N_C!} \int d\vec{r}^{N_c} d\vec{r} \exp\left[-(U(\vec{r}^{N_c}) + \Psi(\vec{r}^{N_c}, \vec{r}))/kT\right] \tag{94}$$

In eq. (94) $U(\vec{r}^{N_c})$ is the interaction, strictly speaking the potential of mean force ($\Delta W(\vec{r}^{N_c}; \mu_o)$ in section 3), between the colloidal particles in the solvent and $\Psi(\vec{r}^{N_c}, \vec{r})$ denotes the interaction between the added polymer molecule and the colloidal particles. Realizing that within the present model

$$\begin{aligned} \exp\left[-\Psi(\vec{r}^{N_c}, \vec{r})/kT\right] &= 0 \quad \text{if the polymer molecule overlaps with} \\ &\quad \text{any of the colloidal particles} \\ &= 1 \quad \text{if there is no overlap} \end{aligned} \tag{95}$$

the integration over the translational polymer degrees of freedom may be performed exactly resulting in

$$Z(N_C, 1, V) = \frac{1}{N_C!} \int d\vec{r}^{N_c} \exp\left[-(U(\vec{r}^{N_c})/kT\right] V_{free}(\vec{r}^{N_c}) \tag{96}$$

In this expression V_{free} is the free volume in which the polymer molecules can move. Clearly this free volume depends on the configuration $\vec{r}^{N_c}$ of the colloidal particles.

Since the polymer molecules do not interact with each other the colloid-polymer interaction between N_C colloidal particles and N_p polymer molecules can be written as a sum of N_p colloid-single polymer interaction terms

$$\Psi(\vec{r}^{N_C}, \vec{r}^{N_P}) = \sum_{j=1}^{N_p} \Psi(\vec{r}^{N_C}, \vec{r}_j) \tag{97}$$

This allows us to write the canonical partition function for N_C colloidal particles and N_p polymer molecules as

$$Z(N_C, N_p, V) = \frac{1}{N_C!}\frac{1}{N_p!}\int d\vec{r}^{N_c} \exp\left[-(U(\vec{r}^{N_c})/kT\right]\left[V_{free}(\vec{r}^{N_c})\right]^{N_p} \tag{98}$$

Substituting this result in eq. (91) we obtain

$$\Xi(N_C, \mu_p, V) = \frac{1}{N_C!}\int d\vec{r}^{N_c} \exp\left[-(W(\vec{r}^{N_c})/kT\right] \tag{99}$$

where W is the *potential of mean force* given by

$$W(\vec{r}^{N_C}) = U(\vec{r}^{N_C}) - kTz_pV_{free}(\vec{r}^{N_C}) \tag{100}$$

Since we treat the polymer as a suspension of non-interacting coils

$$z_p = n_p^r \tag{101}$$

and

$$\Pi_p^r = n_p^r kT \tag{102}$$

Thus the potential of mean force can be written as

$$W(\vec{r}^{N_C}) = U(\vec{r}^{N_C}) - \Pi_p^r V_{free}(\vec{r}^{N_C}) \tag{103}$$

The effective potential W has a many body nature since a full expression for V_{free} can be written only in terms of the mutual overlap of the excluded volume shells of all the colloidal particles. The meaning of the final term in eq. (103) is clearly the following: if the free volume decreases due to a change in the positions of the colloidal particles work has to be done against the osmotic pressure of the reservoir leading to an increase of W. Similarly an increase of the free volume leads to a decrease of W. Note that the second term in eq. (103) is of a purely entropic origin.

To make progress, we use a Van der Waals-mean field approximation [63] and replace $V_{free}(\vec{r}^{N_C})$ in eq. (103) by its average value in the corresponding unperturbed system of colloidal particles.

$$\begin{aligned} \left\langle V_{free}(\vec{r}^{N_C}) \right\rangle &= \frac{\int d\vec{r}^{N_c} V_{free}(\vec{r}^{N_C}) \exp\left[-(U(\vec{r}^{N_c})/kT\right]}{\int d\vec{r}^{N_c} \exp\left[-(U(\vec{r}^{N_c})/kT\right]} \\ &= fV \end{aligned} \tag{104}$$

Obviously it is hard to justify the Van der Waals approximation in the present case, but it is known that this approach leads to good results for the liquid-solid transition of simple atomic systems such as argon[64]. The free volume fraction f depends on the colloid volume fraction ϕ_C and on the relative sizes of colloidal particles and polymer molecules. Using eq. (103) with the approximation (104) to evaluate the grand canonical partition function (99) we obtain

$$\Xi(N_C, \mu_p, V) = \exp\left[\frac{\Pi_p^r fV}{kT}\right] Z_C(N_C, V) \tag{105}$$

where $Z_C(N_C, V)$ is the canonical partition for the pure colloid. From eq. (105) we obtain for the grand potential

$$\Omega = F_C(N_C, V) - \Pi_p^r fV \tag{106}$$

where $F_C(N_C, V)$ is the Helmholtz free energy for the pure colloid. Realizing that the last term on the right hand side of eq. (106) is just the grand potential for a pure polymer solution with chemical potential μ_p and volume fV we can write

$$\Omega = F_C(N_C, V) + \Omega_p(\mu_p, fV) \tag{107}$$

The grand potential thus decouples into a term corresponding to N_C colloidal particles in a volume V and a term corresponding to a pure polymer solution with chemical potential μ_p and volume fV. Eq. (107) can also be transformed in an expression for the Helmholtz free energy that has a similar suggestive form

$$\begin{aligned} F &= \Omega + N_p\mu_p \\ &= F_C(N_C, V) + F_p(N_p, fV) \end{aligned} \tag{108}$$

The chemical potential of the colloid, the osmotic pressure and the number of polymer molecules in the colloid-polymer mixture can be obtained by

differentiation

$$\mu_C = \left(\frac{\partial\Omega}{\partial N_C}\right)_{\mu_p,V} = \mu_C^o - \Pi_p^r \frac{df}{dn_C} \quad (109)$$

$$\Pi = -\left(\frac{\partial\Omega}{\partial V}\right)_{N_C,\mu_p} = \Pi_C^o - \Pi_p^r (f - n_C \frac{df}{dn_C}) \quad (110)$$

$$N_p = -\left(\frac{\partial\Omega}{\partial \mu_p}\right)_{N_C,V} = fV\frac{\partial \Pi_p}{\partial \mu_p} = fVn_p^r \quad (111)$$

Here μ_C^o and Π_C^o denote the chemical potential and the osmotic pressure for the pure colloidal dispersion.

To calculate the phase behaviour we need to solve the coexistence conditions

$$\mu_C'(\phi_C') = \mu_C''(\phi_C'') \quad (112)$$

$$\Pi'(\phi_C') = \Pi''(\phi_C'') \quad (113)$$

at given osmotic pressure $\Pi_p^r = n_p^r kT$. The polymer concentrations in the coexisting phases are then found by using eq. (111)

$$n_p' = f(\phi_C')n_p^r \quad (114)$$

$$n_p'' = f(\phi_C'')n_p^r$$

The present formalism provides a suitable theoretical framework to study systematically the influence of free, non-adsorbing polymer on phase equilibria in colloidal dispersions. Expressions for the Helmholtz free energy $F_C(N_C, V)$ in the pure colloidal system and for the free volume fraction f, are required as an input.

8. Rod-polymer Mixtures: Theory

In order to calculate the influence of added polymer on the phase behaviour of rodlike particles, the Helmholtz free energy $F_C(N_C, V)$ of the pure rod system and the free volume fraction $f = < V_{free} > /V$ have to be known as a function of the density, in the isotropic as well as in the nematic phase. Onsager's second virial theory [3] provides an expression for $F_C(N_C, V)$ and has recently been used in an attempt to treat rod-polymer mixtures, in combination with a geometric approach to calculate $< V_{free} >$ [65]. As discussed in section 4 the use of the Onsager free energy is justified in systems of slender, rigid hard rods as, in the limit of infinite axial ratios, the third and higher virial contributions become vanishingly small compared to the second virial contribution. Adding polymer, however, induces an effective attraction between the rods which (strongly) lowers the second

virial coefficient. Furthermore, some weak inter-rod attraction may have a considerable influence on the third virial coefficient while not affecting significantly the second virial coefficient [66]. Consequently, it is imperative to use a Helmholtz free energy expression which includes, at least approximately, virial contributions beyond the second virial contribution. One such an expression is derived from scaled particle theory [67] for a system of spherocylinders (consisting of cylinders with length L and diameter D, capped by hemispheres of the same diameter).

$$\frac{F_C}{N_C kT} = constant + \ln n_C - \ln(1-\phi_C) + \sigma[f] + \Pi_2 \frac{\phi_C}{1-\phi_C} + \frac{1}{2}\Pi_3 \left(\frac{\phi_C}{1-\phi_C}\right)^2 \tag{115}$$

where

$$n_C = \frac{N_C}{V}$$

$$\phi_C = N_C\left(\frac{\pi}{6}D^3 + \frac{\pi}{4}D^2 L\right)$$

$$\Pi_2 = 3 + \frac{3(\gamma-1)^2}{(3\gamma-1)}\rho[f] \tag{116}$$

$$\Pi_3 = \frac{12\gamma(2\gamma-1)}{(3\gamma-1)^2} + \frac{12\gamma(\gamma-1)^2}{(3\gamma-1)^2}\rho[f] \tag{117}$$

$$\rho[f] = \frac{4}{\pi}\int\int |\sin\gamma| f(\theta) f(\theta') d\Omega d\Omega' \tag{118}$$

$$\sigma[f] = \int f(\theta)\ln[4\pi f(\theta)] d\Omega \tag{119}$$

$$\gamma = \frac{L+D}{D} = \frac{L}{D} + 1.$$

The free energy $F_C = F_C(N_C, V, [f])$ is now a functional of the orientational distribution function $f(\theta)$ so that it accommodates isotropic and nematic phases. In the isotropic phase, $f(\theta) = 1/4\pi$ through normalization and, consequently, $\rho[f] = 1$ and $\sigma[f] = 0$.

In order to calculate the free volume accessible to a polymer with diameter σ_p in a sea of N_C spherocylinders with length L and diameter D in a volume V, we write the chemical potential μ_p of the polymer as follows:

$$\mu_p = \mu_p^+(T) + kT\ln\frac{N_p}{V} + W \tag{120}$$

Here W stands for the reversible work required to introduce the polymer molecule into the pure rod system. On the other hand, according to

Widom's insertion method [63],

$$\mu_p = \mu_p^+(T) + kT \ln \frac{N_p}{< V_{free} >} = \mu_p^+(T) + kT \ln \frac{N_p}{V} - kT \ln f \quad (121)$$

By combining eq. (120) and eq. (121), we find that

$$W = -kT \ln f$$

so that

$$f = \exp\left(-\frac{W}{kT}\right) \quad (122)$$

Using the scaled particle theory to calculate W, the following expression for the free volume fraction is obtained:

$$f = (1-\phi_C) \exp\left[-\left\{A\left(\frac{\phi_C}{1-\phi_C}\right) + B\left(\frac{\phi_C}{1-\phi_C}\right)^2 + C\left(\frac{\phi_C}{1-\phi_C}\right)^3\right\}\right] \quad (123)$$

where

$$q = \frac{\sigma_p}{D}$$

$$A = \frac{6\gamma}{3\gamma-1}q + \frac{3(\gamma+1)}{3\gamma-1}q^2 + \frac{2}{3\gamma-1}q^3 \quad (124)$$

$$B = \frac{1}{2}\left(\frac{6\gamma}{3\gamma-1}\right)^2 q^2 + \left(\frac{6}{3\gamma-1} + \frac{6(\gamma-1)^2}{(3\gamma-1)}\rho[f]\right) q^3 \quad (125)$$

$$C = \frac{2}{3\gamma-1}\left(\frac{12\gamma(2\gamma-1)}{(3\gamma-1)^2} + \frac{12\gamma(\gamma-1)^2}{(3\gamma-1)^2}\rho[f]\right) q^3 \quad (126)$$

We can now proceed to calculate the phase behaviour of rod-polymer mixtures by first minimizing $\Omega(N_C, V, \Pi_p^r, [f])$ with respect to the orientional distribution function:

$$\frac{\partial \Omega}{\partial f} = 0 \quad (127)$$

In practice we used a Gaussian trial function [49]

$$f(\theta) \sim \left(\frac{\alpha}{4\pi}\right) \exp\left(-\frac{1}{2}\alpha\theta^2\right) \qquad 0 \le \theta \le \frac{\pi}{2} \quad (128)$$

$$\sim \left(\frac{\alpha}{4\pi}\right) \exp\left(-\frac{1}{2}\alpha(\pi-\theta)^2\right) \qquad \frac{\pi}{2} \le \theta \le \pi$$

the variational parameter α being determined by the condition that

$$\frac{\partial \Omega}{\partial \alpha} = 0 \tag{129}$$

Subsequently, we solved the coexistence conditions

$$\mu'_C(\phi'_C,[f']) = \mu''_C(\phi''_C,[f'']) \tag{130}$$

$$\Pi'(\phi'_C,[f']) = \Pi''(\phi''_C,[f'']) \tag{131}$$

using the scaled-particle results for the Helmholtz free energy (115) and the free volume fraction (123). The former leads to the following expressions for the pure rod chemical potential μ^0_C and pressure Π^0_C, which are to be used in (109) and (110) respectively:

$$\frac{\Pi^0_C}{n_C kT} = \frac{1}{1-\phi_C} + \Pi_2 \frac{\phi_C}{(1-\phi_C)^2} + \Pi_3 \frac{\phi_C^2}{(1-\phi_C)^3} \tag{132}$$

$$\frac{\mu^0_C}{kT} = \frac{\mu^+_C(T)}{kT} + \ln n_1 - \ln(1-\phi_C) + (1+2\Pi_2)\frac{\phi_C}{1-\phi_C} + \left(\Pi_2 + \frac{3}{2}\Pi_3\right)\left(\frac{\phi_C}{1-\phi_C}\right)^2 + \Pi_3\left(\frac{\phi_C}{1-\phi_C}\right)^3 \tag{133}$$

The procedure of solving (130,131) together with (129) was repeated for a wide range of "geometries", fixed by the L/D-ratio of the spherocylinders and the relative size $q = \sigma_p/D$ of the polymer molecules. For each {L/D,q}-combination, the phase equilibria had to be evaluated at different Π^r_p-values (or, equivalently, ϕ^r_p or $\mu^r_p = \mu_p$ values), $\Pi^r_p = 0$ corresponding to the pure rod limit. From the calculations it follows that rod-polymer mixtures may exhibit 3 types of phase behaviour.

I: two isotropic phases (diluted and concentrated) and a single nematic phase. (Fig. 19a,20a). This behaviour is observed in mixtures of relatively short rods and large polymers.

II: an isotropic and a nematic phase, in intermediate cases. (Fig. 19b,20b)

III: an isotropic phase and two nematic phases (diluted and concentrated). (Fig. 19c,20c) This behaviour is typical for mixtures of long rodlike particles and comparatively small polymer molecules.

The occurrence of the 3 different regimes as a function of the geometrical parameters L/D and q, is shown in Fig. 21.

9. Rod-Polymer Mixtures: Experiments

9.1. INTRODUCTION

Here we describe experiments on phase transitions in mixed dispersions consisting of sterically stabilized rod-like colloidal boehmite particles and a

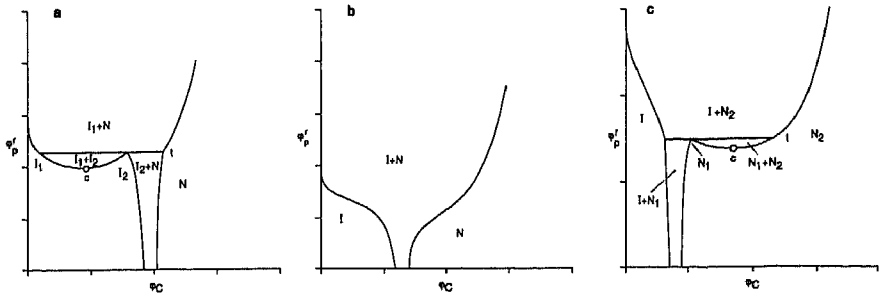

Figure 19. Schematic representation of phase diagrams for rod-like colloid-flexible polymer mixtures showing colloid volume fraction ϕ_C against polymer volume fraction in the reservoir ϕ_p^r for a) small σ_p/D, b) intermediate σ_p/D c) large σ_p/D. Tie lines are shown in the two-phase regions. The isotropic phase is indicated by I (or I_1 and I_2 in the case of two isotropic phases) and the nematic phase by N (or N_1 and N_2 in the case of two nematic phases. In a) and c) the critical point (c) and triple line (t) are also indicated.

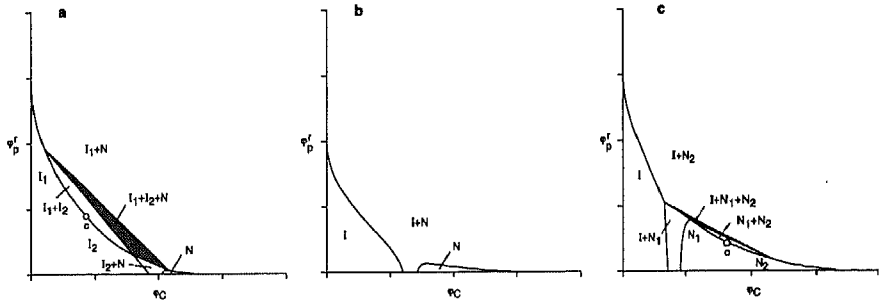

Figure 20. Schematic representation of phase diagrams for rod-like colloid-flexible polymer mixtures showing colloid volume fraction ϕ_C against polymer volume fraction in the system ϕ_p. The notation is the same as in figure 19. Note that the oblique tie lines imply considerable partitioning of the polymer among the phases. In the (ϕ_C, ϕ_P)-plane the triple lines observed in a) and c) become regions of three phase coexistence.

flexible polymer (polydimethylsiloxane or polystyrene). The effect of flexible polymer on dispersions of rod-like colloidal particles was already observed over fifty years ago by Cohen [68] who studied the isolation and crystallization of plant viruses (such as Tobacco Mosaic Virus) by means of the addition of heparin. He observed that the addition of less than 0.5% heparin to a dispersion of TMV leads to a precipitate of the virus particles. In the sixties this effect was rediscovered [69] with polyethyleneglycol as precipi-

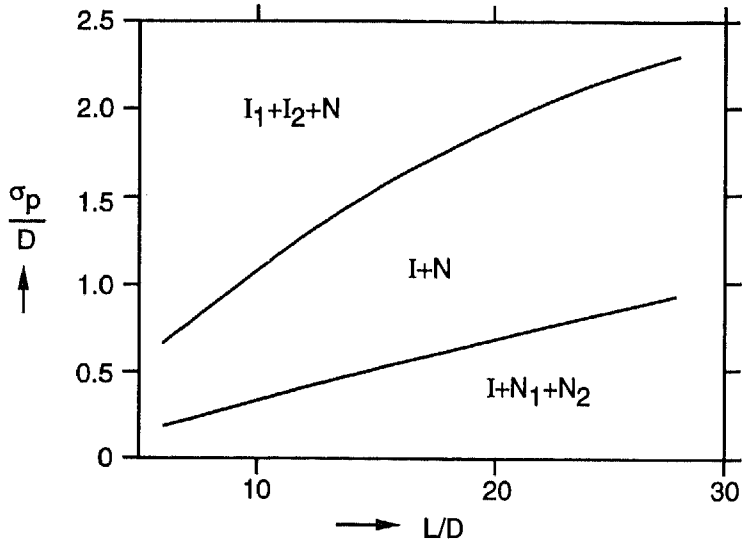

Figure 21. Dependence of the type of phase behaviour of rod-like colloid-flexible polymer mixtures on the size parameters of the colloid and polymer.

tating agent and was subsequently used for the isolation and purification of virus particles [70-72]. As the emphasis in this work was on isolation and purification of virus particles limited attention was paid to the fundamental phase equilibrium aspects underlying the process. Also closely related to the experiments described here is the study of phase equilibria in ternary systems consisting of a rigid polymer, a flexible polymer and a solvent [73-75].

9.2. MATERIALS

Colloidal rods: Polyisobutene grafted boehmite rods [43].
PDMS: Polydimethylsiloxane, used with the cyclohexane dispersions (ASBIP13g).
PS: Polystyrene, used with the o-dichlorobenzene dispersions (ASB33g).

9.3. RESULTS

9.3.1. *Rods with a Length to Width Ratio of 6.4 (ASB33g)*

The phase behaviour for the ASB33g system is studied with 35k PS as added polymer. Several coexisting phases are observed for this system, of

TABLE 3. Characterization of the colloidal rods

	ASBIP13g	ASB33g
Average length (nm)	253[a]	71
Standard deviation of the length (nm)	-	31
Average width (nm)	9.4[a]	11.1
Standard deviation of the width (nm)	-	2.4
Correlation coefficient	-	0.40
Average particle density (g cm^{-3})	2.11 ± 0.07	1.97 ± 0.07

[a] Best estimate

TABLE 4. Characterization of the polymer samples

Polymer	$M_w(gmol^{-1})$	M_w/M_n	$< R_g^2 >^{1/2}$ (nm)		$\sigma_p(nm)$[a]
			q − solvent	*used solvent*	
PDMS	65000	1.49	6.8	10.5	24
PDMS	92000	1.30	8.1	13	29
PDMS	186000	-	11.5	20	45
PS	35000	< 1.06	5.2	5.9	13.3

[a] The polymer diameter σ_p is obtained by multiplying the radius of gyration with 2.25. [76]

which the most important are a dilute isotropic (gas-like) phase (I_1), a concentrated isotropic (liquid-like) phase (I_2), and a birefringent (nematic-like) phase (N). On tilting the sample tube both isotropic phases flow immediately, while it takes the nematic phase about 15 to 60 minutes to flow completely. Almost all phase separations are completed within two days. An example of a I_1 I_2 N three phase equilibrium is shown in fig. 22.

An overview of the results is shown in the phase diagram in fig. 23. Apart from the coexisting phases already discussed, some additional states are observed. On increasing the polymer concentration first a relatively colorless and turbid amorphous sediment separates from the dispersion, which can be ascribed entirely to clusters (C) that are present in the boehmite dispersions (to be discussed later). The other additional states are found when we follow the dilution line which starts at $\phi_{rod} = 23.4$v/v% and [PS] = 28.4 g/l and goes towards the origin of the plot. At the starting point a gel-like, sticky and very turbid dispersion is obtained after thoroughly mixing the sample. Subsequent phase separation results in an upper phase with a very low boehmite concentration (< 0.75v/v%) and a turbid gel or glass-like (G)

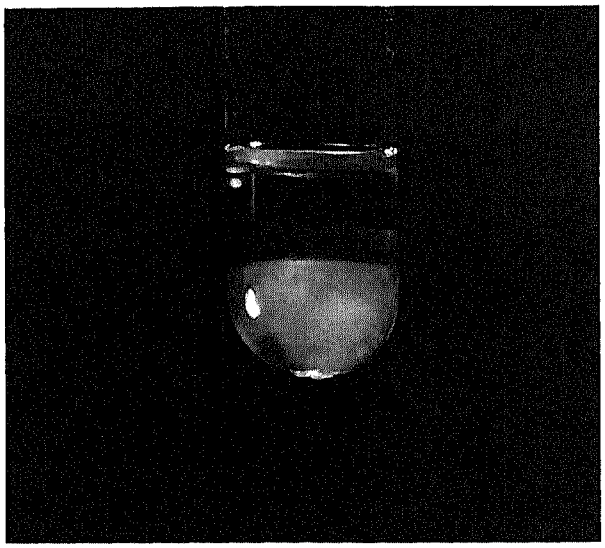

Figure 22. Photograph of the ASB33g sample with ϕ_{rod} = 20.6% and a polystyrene concentration of 18.0 g/l. The sample is placed between crossed polars. To make the two isotropic phases visible the sample is illuminated from the side.

lower phase that does not flow within an hour after tilting the sample tube. Neglecting the boehmite in the upper phase, the boehmite concentration in the lower phase can be estimated to be approximately 33v/v%.

Diluting the sample to ϕ_{rod} = 18.8v/v% and [PS] =22.9 g/l again results in an upper phase with a very low boehmite concentration, but now the lower phase is birefringent. This lower phase does not flow within one hour and is therefore denoted as a nematic glass (N_g). Its concentration is about 38v/v%.

Upon further dilution, the boehmite concentration in the upper phase increases and the lower phase starts to flow and develops a finer and sharper birefringence pattern. At the point where the lower phase first flows completely within one hour after tilting the sample tube, it is denoted as a nematic (N). At this point the boehmite concentration in the upper phase is estimated to be 2 ± 0.5v/v%. Further diluting till the boundary of the three phase region, the upper phase reaches a boehmite concentration of 3.5 ± 1v/v%.

A remarkable change is observed on going through the three phase region. In the upper half of the three phase region, the main change in the

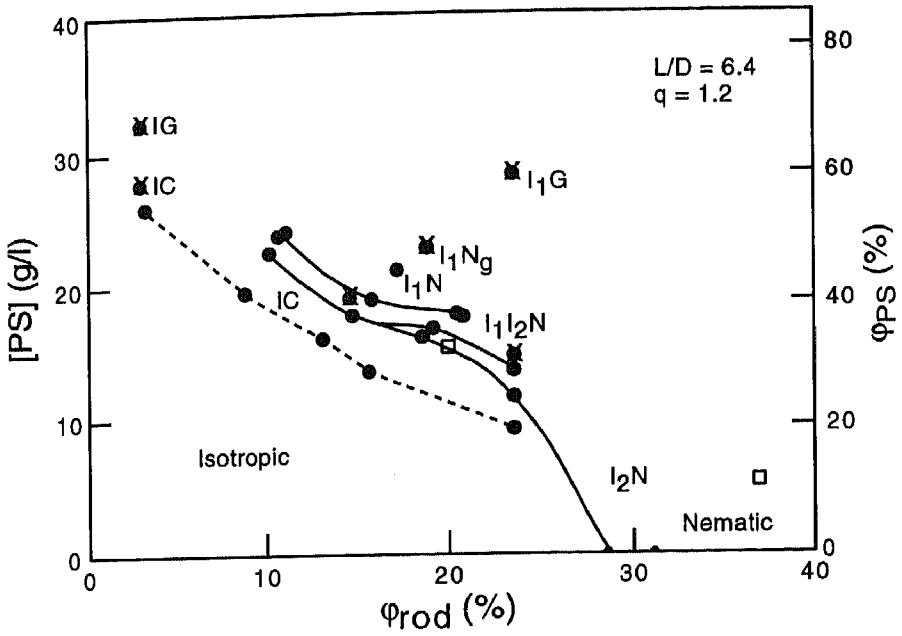

Figure 23. Observed phases for ASB33g dispersions in o-dichorobenzene with 35k PS added, plotted as a function of the boehmite volume fraction ϕ_{rod} and the polymer concentration, which is given in g/l as well as the effective sphere volume fraction. Different phases and states are denoted as: I isotropic, N nematic, G glass or gel, N_g "nematic" (i.e. birefringent) glass or gel, and C cluster sediment. The solid dots denote measured phase boundaries the asterisks denote single samples or starting points of a dilution series, and the open squares denote the estimated coexisting phases for the sample with ϕ_{rod} = 23.4% and [PS]=13.3 g/l. The drawn lines are cubic spline fits for the major phase boundaries, and the dotted line connects limiting concentrations for a cluster sediment (IC coexistence).

sample is that the amount of I_2 phase increases and the amount of N phase decreases. In the lower half of the three phase region, however, the main change is in the concentrations of the I_1 and I_2 phase, which are approaching each other, together with a slow decrease of that what remained of the nematic phase. This scenario is typical for dilution in the three phase region, except for the vertical dilution line at ϕ_{rod} = 23.4v/v%. There the concentration of I_1 remains 3 ± 1v/v%, and only the amount of I_1 decreases until the I_2 N region is entered.

9.3.2. *Rods with a Length to Width Ratio of about 27 (ASBIP13g)*
Phase separation experiments were performed for 65, 92 and 186 kg mol^{-1} PDMS samples (table 4), with boehmite concentrations up to the isotropic-nematic phase separation. After the addition of a sufficient amount of polymer and thoroughly mixing the sample, a phase separation, in a turbid concentrated and a more clear dilute phase, occurs within a few hours to a few days. The concentrated phases have a rigid structure, which takes a few minutes to a few hours to flow completely after tilting a sample tube. In contrast the isotropic-nematic phase separation without added polymer produces phases that flow quickly after tilting the sample tube (even the more viscous nematic phase flows completely within 10s). It is remarkable that some of the concentrated phases are birefringent and others are not. The concentrated phases for the samples with the 186k PDMS are birefringent, whereas the samples with the 65k and the 92k PDMS do only give birefringent concentrated phases at the highest boehmite concentration used (5.3v/v%). On average, the birefringent concentrated phases flow a little faster and are somewhat less turbid than the non-birefringent concentrated phases.

The limiting polymer concentrations (c_{lim}) for phase separation are given in fig. 24. It is found that the polymer concentration needed for phase separation decreases with increasing molar mass as well as with an increasing volume fraction of the rods. This general behaviour is similar to depletion phase separation of spherical colloid-flexible polymer mixtures. Note that the description of the concentrated phases given in the last paragraph applies to polymer concentrations which are just above c_{lim}

An interesting observation was made on a sample with a somewhat higher polymer concentration. Here the concentrated coexisting phase is formed from an initial gel-like lower phase with a large volume which then shrinks to a much smaller volume. This is in contrast to the usual case, where the relatively small volume of the concentrated phase forms directly out of the dilute phase (like sediment formation). This observation seems similar to the phenomenon described in a recent work on the gel state in depletion experiments with colloidal spheres at high polymer concentration [77].

9.4. DISCUSSION AND COMPARISON TO THEORY

9.4.1. *Rods with a Length to Width Ratio of 6.4*
The phase diagram calculated with the theory presented in section 8 with the parameters relevant for the system consisting of boehmite rods ASB33g ($\gamma = (L+D)/D = 6.4$) with 35k PS ($q = \sigma_p/D = 1.2$) is given in figure 25a. The correspondence with the experimental results presented in figure 23

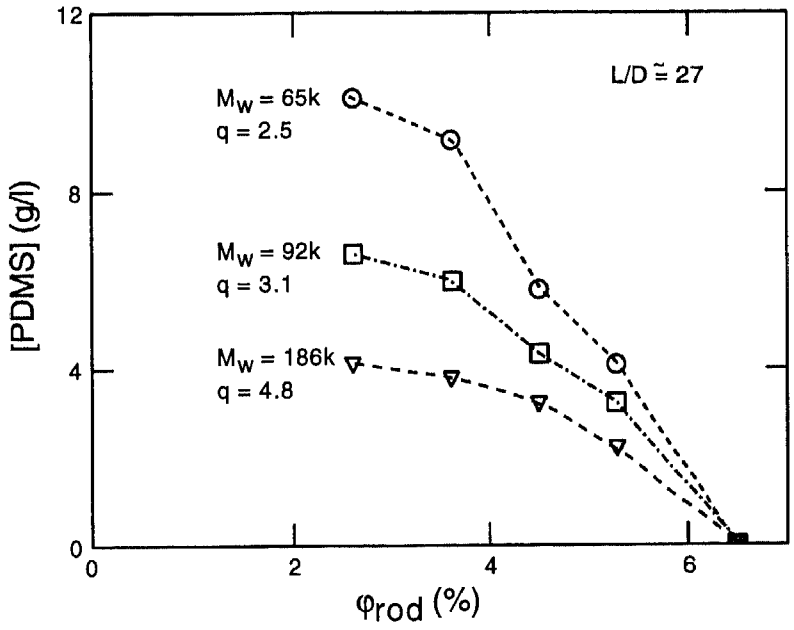

Figure 24. Limiting polymer concentrations for phase separation of the ASBIP13g sample in cyclohexane with polydimethylsiloxane as polymer. The different structures of the coexisting concentrated phases are discussed in the text.

is poor. This disagreement may be explained by polydispersity effects in the system and approximations in the theory. However, simply assuming a smaller effective polymer diameter already gives a much better agreement between theory and experiment as is evident from the theoretical phase diagram for $\gamma = 6.4$ and q=0.8 presented in figure 25b.

On following a dilution line through the three phase $I_1 I_2 N$ region, it is observed experimentally that the I_1 and I_2 concentrations approach each other in the lower half of the three phase region. Although this behaviour would be expected in the I_1 I_2 region, in the three phase region the concentrations of the coexisting phases should remain constant, while the volumes of the phases change. This provides evidence for the fact that the polydispersity of the rods, like in the case of the pure rod dispersion (section 6), again plays an important role in the phase behaviour. In order to understand why this leads to the disappearance of the $I_1 I_2$ region from the phase diagram requires a calculation in which the polydispersity of the rods is taken into account by representing them at least as a bidisperse system.

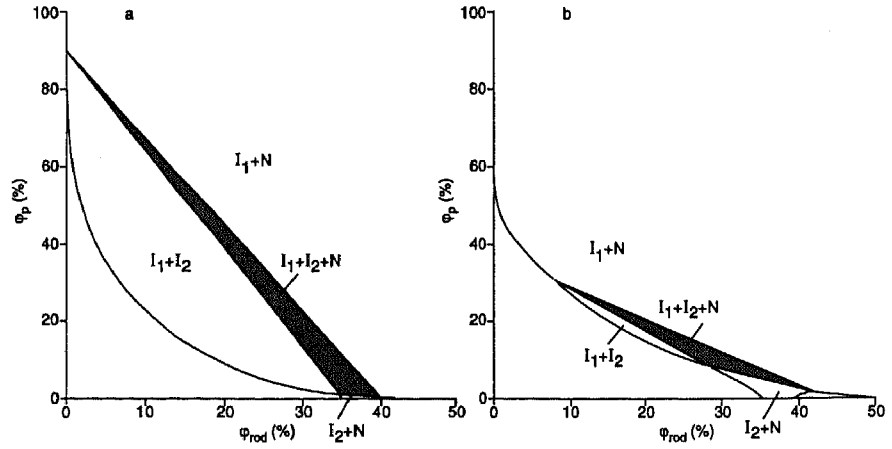

Figure 25. Theoretical phase diagrams for a system of rod-like colloidal particles and flexible polymers. a) $\gamma = 6.4$ and $q = 1.2$ b) $\gamma = 6.4$ and $q = 0.8$.

Judging from the success this had in the case of the pure rod-like system it appears worthwhile to undertake such calculations.

In addition to the isotropic and nematic phases, gel or glass states, not considered in the theory, are found at high polymer concentrations. This behaviour resembles (some of) the results in a recent study on the gel state in colloidal sphere/polymer mixtures [77,78]. Apparently, at high polymer concentrations the attractions are too strong to allow the system to reach its equilibrium state. This might also explain the change from a gel or glass which appears non-birefringent at the highest polymer concentration, to a birefringent "nematic" gel or glass state at somewhat lower polymer concentrations. Finally at still lower polymer concentrations a flowing birefringent (nematic) phase is observed.

9.4.2. *Rods with a Length to Width Ratio of 27*

The phase diagrams calculated using the theory presented in section 8 with the parameters relevant for the system consisting of boehmite rods ASBIP13g (γ= (L+D)/D = 27) with 65k, 92k and 186k PDM ($q = \sigma_p/D = 2.5$, 3.1 and 4.8) are presented in figure 26.

To facilitate the comparison between theory and experiment the experimental results given in figure 24 are replotted in figure 27 where the polymer concentration is given as the volume fraction of the effective polymer spheres (ϕ_{PDMS}). Clearly, the phase behaviour predicted by theory shows significant discrepancies with the experimental results. In addition

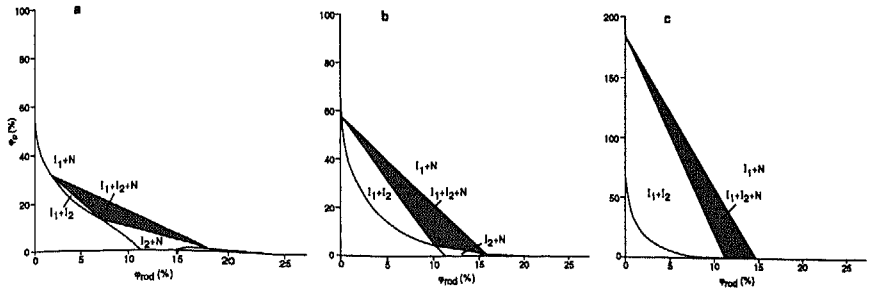

Figure 26. Theoretical phase diagrams for a system of rod-like colloidal particles and flexible polymers. a) $\gamma = 27$ and q=2.5, b) $\gamma = 27$ and q=3.1, c) $\gamma = 27$ and q=4.8.

to the effect of polydispersity of the rods, not taken into account in the theory, the large difference between theoretical and experimental phase behaviour is probably due to limitations in the theory to deal with systems where the polymer diameter is significantly larger than the rod diameter. As a consequence the $I_1 I_2$ region is seriously overestimated in the theoretical phase diagrams. Like in the case of the ASB33g system assuming a smaller effective polymer diameter would already give a much better agreement between theory and experiment.

Another factor that we have to take into account is the formation of gel or glass states. As indicated under the experimental results, the concentrated phases for the boehmite dispersions to which the 186k PDMS is added are birefringent, whereas the boehmite dispersions to which 65k or 92k PDMS is added only give birefringent concentrated phases at the highest boehmite concentration. Given the fact that rod-like colloidal particles have a strong tendency to cluster under the influence of attractive forces a possible explanation for the experimental observation is that in the case of 65k and 92k PDMS the attractive depletion potential is so narrow and deep as to give rise to clusters that do not have the capability to rearrange to a nematic ordering. Whereas it appears that in the case of 186k PDMS the attractive well is sufficiently broad to allow for nematic ordering. However, this is pure speculation and whether the concentrated phases have a glass or gel structure awaits further experimental evidence.

Acknowledgements

We thank Mrs. Marina Uit de Bulten and Mrs. Hanneke de Vries for preparing the manuscript and Mr. J. den Boesterd for making the drawings and photographs.

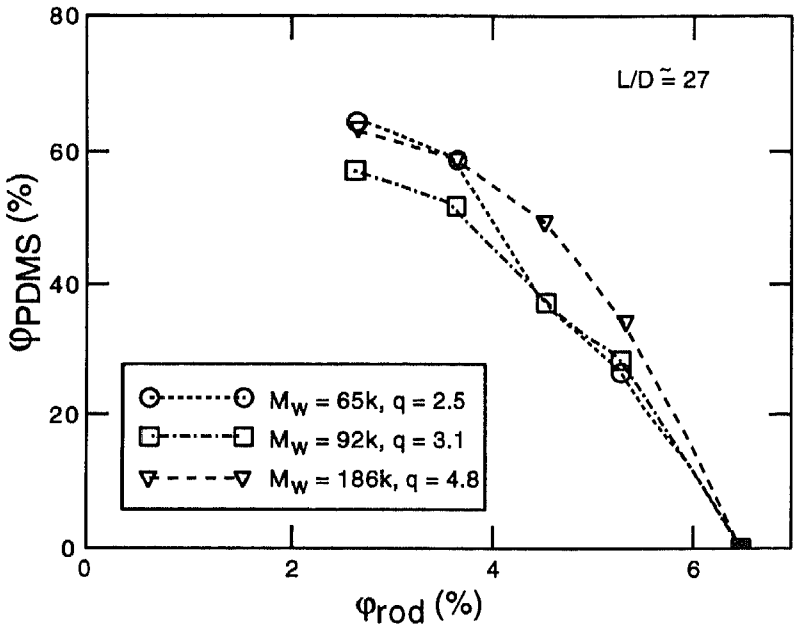

Figure 27. Experimental phase diagrams from fig. 22 replotted as a function of the effective polymer volume fraction ϕ_{PDMS}.

General References

These lectures are largely based on the work described in:

- G.J. Vroege and H.N.W. Lekkerkerker, Theory of the isotropic-nematic-nematic phase separation for a solution of bidisperse rodlike particles. J. Phys. Chem. 97 (1993) 3601.
- P.A. Buining and H.N.W. Lekkerkerker, Isotropic-nematic phase separation of a dispersion of organophilic boehmite rods. J. Phys. Chem. 97 (1993) 11510.
- H.N.W. Lekkerkerker and A. Stroobants, The phase behaviour of colloid-polymer and colloid-colloid mixtures. Lecture Notes in Physics 415, Complex Fluids. (Ed. L. Garrido, Springer Verlag, Berlin 1993). 1.
- A. Stroobants and H.N.W. Lekkerkerker, Phase behaviour of rod-like colloid+flexible polymer mixtures, submitted for publication to Macromolecules.

- J. Buitenhuis, L.N. Donselaar, P.A. Buining and H.N.W. Lekkerkerker, Phase separation of mixtures of colloidal boehmite rods and flexible polymer, submitted for publication to J. Colloid Interface Sci.

References

1. Onsager, L. (1933) *Chem. Rev.* **13**, 73.
2. Onsager, L. (1942) *Phys. Rev.* **62**, 558.
3. Onsager, L. (1949) *Ann. N.Y. Acad. Sci.* **51**, 627.
4. McMillan, W.G. and Mayer, J.E. (1945) *J. Chem. Phys.*,**13**, 276.
5. Derjaguin, B.V. and Landau, L.D. (1941) *Acta Physicochimica URSS*,**14**, 633.
6. Verwey, E.J.W. and Overbeek, J.Th.G. (1948) *Theory of the stability of lyophobic colloids*, Elsevier, Amsterdam.
7. Frens, G. and Overbeek, J.Th.G. (1972) *J. Colloid Interface Sci.* **38**, 376.
8. Sciortino, F. and Tartaglia, P. (1994), *preprint.*
9. Luck, W., Klier, M. and Wesslau, H. (1963) *Ber. Bunsenges. Phys. Chem.* **67**, 75.
10. Hiltner, P.A. and Krieger, I.M. (1969) *J. Phys. Chem.* **73**, 2386.
11. Hachisu, S., Kobayashi, Y. and Kose, A. (1973) *J. Colloid Interface Sci.* **42**, 342 and (1974), **46**, 470.
12. Kirkwood, J.G. (1939) *J. Chem. Phys.* **7**, 919.
13. Wood, W.W. and Jacobson, J.D. (1958) *J. Chem. Phys.* **27**, 1207.
14. Alder, B.J. and Wainwright T.E. (1958) *J. Chem. Phys.* **27**, 1208.
15. Hoover, W.G. and Ree, F.H. (1968) *J. Chem. Phys.* **49**, 3609.
16. Wadati, M. and Toda, M. (1972) *J. Phys. Soc. Japan*, **32**, 1147.
17. Antl, L., Goodwin, J.W., Hill, R.D., Ottewill, R.H., Owens, S.W., Papworth, S. and Waters J.A. (1986) *Colloids and Surfaces*, **17**, 67.
18. Helden, A.K. van, Jansen, J.W. and Vrij A. (1981) *J. Colloid Interface Sci.* **81**, 354.
19. Pusey, P.N. and van Megen, W. (1986) *Nature*, **320**, 340.
20. Zocher, H. (1925) *Z. Anorg. Chem.* **147**, 91.
21. Bawden, F.C., Pirie, N.W., Bernal, J.D. and Fankuchen, I. (1936) *Nature* **138**, 1051.
22. Bawden, F.C. and Pirie, N.W., (1937) *Proc. Roy. Soc. B* **123**, 274.
23. Bernal, J.D. and Fankuchen, I. (1941) *J. Gen. Physiol.* **25**, 111.
24. Langmuir, I. (1938) *J. Chem. Phys.* **6**, 873.
25. Best, R.J. (1939) *J. Austral. Inst. Agric. Sci.* **5**, 94.
26. Hansen, J.P. and McDonald, I.R. (1986) *Theory of Simple Liquids*, Academic Press, New York.
27. Long, J.A., Osmond, D.W.J. and Vincent, B. (1975) *J. Colloid Interface Sci.* **42**, 545.
28. Martinov, G.A. and Muller, V.M. (1974) *Coll. J. USSR*,**36**, 631.
29. Vrij, A. (1976) *Pure & Appl. Chem.* **48**, 471.
30. Victor, J.M. and Hansen, J.P. (1985) *J. Chem. Soc. Faraday Trans II* **81**, 43.
31. Gast, A.P., Hall, C.K. and Russel, W.B. (1983) *J. Colloid Interface Sci.* **96**, 251.
32. Vincent, B.J., Edward, J. Emmett, S. and Croot R. (1988) *Colloids Surf.* **31**, 267.
33. Lekkerkerker, H.N.W., Poon, W.C.K., Pusey, P.N., Stroobants, A. and Warren, P.B. (1992) *Europhys. Lett.* **20**, 559.
34. Hagen, M.H.J., Meijer, E.J., Mooij, G.C.A.M., Frenkel, D. and Lekkerkerker, H.N.W. (1993) *Nature (London)* **365**, 425.
35. Bolhuis, P. and Frenkel D. (1994) *Phys. Rev. Lett.* **72**, 2211.
36. Tejero, C.F., Daanoun, A., Lekkerkerker, H.N.W. and Baus, M. (1994) *Phys. Rev. Lett.* **73**, 752.
37. Kotera, A., Furusawa, K. and Kudo, K. (1970) *Kolloid Z. u. Z. Polymere* **240**, 837.
38. Jansen, J.W., Kruif, C.G. de and Vrij, A. (1986) *J. Colloid Interface Sci.* **114**, 481.
39. Kranendonk, W.G.T. and Frenkel, D. (1988) *Mol. Phys.* **64**, 403.

40. Pusey, P.N., Poon, W.C.K., Ilett, S.M. and Bartlett, P. (1994) *J. Phys.: Condens. Matter* **6**, A29.
41. Buining, P.A., Pathmamanoharan, C., Bosboom, M., Jansen, J.B.H., Lekkerkerker, H.N.W. (1990) *J. Am. Ceram. Soc.* **73**, 2385.
42. Buining, P.A., Pathmamanoharan, C., Jansen, J.B.H., Lekkerkerker, H.N.W. (1991) *J. Am. Ceram. Soc.* **74**, 1303.
43. Buining, P.A., Veldhuizen, Y.S.J., Pathmamanoharan, C., Lekkerkerker, H.N.W. (1992) *Colloid Surfaces* **64**, 47.
44. Perrin, J. (1909) *Ann. de Chim. et de Phys.* **18**, 5.
45. Perrin, J. (1914) *Compt. Rend.* **158**, 1168.
46. Constantin, R. (1914) *Compt. Rend.* **158**, 1171.
47. Pusey, P.N. (1991) Liquids, Freezing and the Glass Transition, in J.P. Hansen, D. Levesque and J. Zinn-Justin (eds.), *Les Houches,Session LI*, Elsevier, Amsterdam, 763.
48. Frenkel, D. (1987) *J. Phys. Chem.* **91**, 4912 (Erratum (1988) *J. Phys. Chem.* **92**, 5314).
49. Odijk, T. (1986) *Macromolecules* **19**, 2313.
50. Lekkerkerker, H.N.W., Coulon, P., Van der Haegen, R. and Deblieck, R. (1984) J. *Chem. Phys.* **80**, 3427.
51. Straley, J.P. (1973) *Mol. Cryst. Liq. Cryst.* **24**, 7.
52. Tjipto-Margo, B. and Evans, G.T. (1990) *J. Chem. Phys.* **93**, 4254.
53. Vroege, G.J. and Lekkerkerker, H.N.W. (1992) *Rep. Progr. Phys.* **55**, 1241.
54. Odijk, T. and Lekkerkerker, H.N.W. (1985) *J. Phys. Chem.* **89**, 2090.
55. Bartlett, P. (1990) *J. Phys.: Condens. Matter* **2**, 4979.
56. Flory, P.J. and Abe, A. (1978) *Macromolecules* **11**, 1119.
57. Birshtein, T.M., Kolegov, B.I. and Pryamitsyn, V.A. (1988) *Vysokomol. Soyed. A* **30**, 348 [(1988) *Polym. Sci. U.S.S.R.* **30**, 316).
58. Pathmamanoharan, C. (1988/89) *Colloids Surfaces* **34**, 81.
59. Asakura, S. and Oosawa, F. (1954) *J. Chem. Phys.* **22**, 1255.
60. Asakura, S. and Oosawa, F. (1958) *J. Polym. Sci.* **23**, 183.
61. Widom, B. and Rowlinson J.S. (1970) *J. Chem. Phys.* **52**, 1670.
62. Meijer, E.J. and Frenkel, D. (1992) *Phys. Rev. Lett.* **67**, 1110.
63. Widom, B. (1963) *J. Chem. Phys.* **39**, 2808.
64. Longuet-Higgins, H.C. and Widom, B. (1964) *Mol. Phys.* **8**, 549.
65. Warren, P.B. (1994) *J. Phys. I. France* **4**, 237.
66. Schoot, P. van der and Odijk, T. (1992) *J. Chem. Phys.* **97**, 515.
67. Cotter, M. (1977) *J. Chem. Phys.* **66**, 1098.
68. Cohen, S.S. (1942) *J. Biol. Chem.* **144**, 353.
69. Herbert, T.T. (1963) *Phytopathology* **53**, 362
70. Venekamp, J.H. and Mosch W.H.M. (1964) *Virology* **22**, 503.
71. Leberman, R. (1966) *Virology* **30**, 341.
72. Yamamoto, K.R., Alberts, B.M., Benzinger, R., Lawthorne, L. and Treiber, G. (1970) *Virology* **40**, 734.
73. Bianchi, E., Ciferri, A., Conio, G., Marsano, E. and Tealdi, A. (1984) *Macromolecules* **17**, 1526.
74. Marsano, E., Bianchi, E., Ciferri, A. Ramis, G. and Tealdi, A. (1986) *Macromolecules* **19**, 626.
75. Russo, P.S. and Cao, T. (1988) *Mol. Crys. Liq. Cryst.* **157**, 501.
76. Hek, H. de and Vrij, A. (1981) *J. Coll. Interface Sci.* **84**, 409.
77. Pusey, P.N., Pirie, A.D. and Poon W.C.K. (1993) *Physica A* **201**, 322.
78. Smits, C., Van der Most, B., Dhont, J.K.G. and Lekkerkerker, H.N.W. (1992) *Adv. Colloid Interface Sci.* **42**, 33.